

---

# ROBUST MULTI-TASK BOOSTING USING CLUSTERING AND LOCAL ENSEMBLING

---

**Seyedsaman Emami**

Escuela Politécnica Superior  
Universidad Autónoma de Madrid  
Madrid

**Daniel Hernández-Lobato**

Escuela Politécnica Superior  
Universidad Autónoma de Madrid  
Madrid

**Gonzalo Martínez-Muñoz**

Escuela Politécnica Superior  
Universidad Autónoma de Madrid  
Madrid

Centro de Investigación Avanzada en Física Fundamental  
Universidad Autónoma de Madrid  
Madrid

## Abstract

Multi-Task Learning (MTL) aims to boost predictive performance by sharing information across related tasks, yet conventional methods often suffer from *negative transfer* when unrelated or noisy tasks are forced to share representations. We propose Robust Multi-Task Boosting using Clustering and Local Ensembling (RMB-CLE), a principled MTL framework that integrates error-based task clustering with local ensembling. Unlike prior work that assumes fixed clusters or hand-crafted similarity metrics, RMB-CLE derives inter-task similarity directly from *cross-task errors*, which admit a risk decomposition into functional mismatch and irreducible noise, providing a theoretically grounded mechanism to prevent negative transfer. Tasks are grouped adaptively via agglomerative clustering, and within each cluster, a local ensemble enables robust knowledge sharing while preserving task-specific patterns. Experiments show that RMB-CLE recovers ground-truth clusters in synthetic data and consistently outperforms multi-task, single-task, and pooling-based ensemble methods across diverse real-world and synthetic benchmarks. These results demonstrate that RMB-CLE is not merely a combination of clustering and boosting but a general and scalable framework that establishes a new basis for robust multi-task learning.

## List of Abbreviations

<b>CD</b>	Critical Distance
<b>CMTL</b>	Clustered Multi-Task Learning
<b>DNN</b>	Deep Neural Network
<b>DP</b>	Data Pooling
<b>GB</b>	Gradient Boosting
<b>LGBM</b>	Light Gradient-Boosting Machine
<b>MAE</b>	Mean Absolute Error
<b>ML</b>	Machine Learning
<b>MLP</b>	Multi-Layer Perceptron
<b>MT</b>	Multi-Task
<b>MTGB</b>	Multi-Task Gradient Boosting
<b>MTL</b>	Multi-Task Learning
<b>RMB-CLE</b>	Robust Multi-Task Boosting using Clustering and Local Ensembling
<b>RMSE</b>	Root Mean Squared Error
<b>R-MTGB</b>	Robust-Multi-Task Gradient Boosting
<b>ST</b>	Single-Task
<b>Std Dev</b>	Standard Deviation
<b>TaF</b>	Task-as-Feature
<b>TS</b>	Task-Specific

## 1 Introduction

Multi-Task Learning (**MTL**) is a key domain in Machine Learning (**ML**) where models are trained to perform several related or unrelated tasks simultaneously, facilitating the transfer of knowledge between tasks [1]. **MTL** aims to strengthen generalization by combining task-specific insights with representations that are shared across multiple tasks [2]. A foundational work in [2] introduced the concept of hard parameter sharing in neural networks for **MTL**, where a single model with multiple output layers learns to solve several tasks concurrently. This setup allows the shared layers to capture representations that are useful across tasks, promoting inductive transfer during training. **MTL** models have numerous real-world applications; for instance, they have been used to simultaneously predict mood and stress levels of patients by leveraging information from the entire population under study [3].

From an algorithmic perspective, **MTL** approaches are often categorized into five families: feature learning [2, 4, 5, 6, 7], low-rank approaches [8, 9, 10], task clustering [11, 12, 13], task relation learning [14, 15, 16], and decomposition methods [17, 18]. Among these, task clustering methods, also known as Clustered Multi-Task Learning (**CMTL**), have been widely explored. **CMTL** assumes that tasks can be grouped into clusters based on their similarity, allowing the model to capture shared structure within task groups while maintaining flexibility across unrelated tasks [19, 1].

In this work, we concentrate on the third family, clustering-based multi-task methods. Clustering, an unsupervised learning method, groups data based on similarity measures [20, 21, 22]. In the context of **CMTL**, clustering is used to group tasks instead of data points. Hierarchical clustering, particularly the agglomerative variant [22], is well-suited for capturing graded relationships between tasks [23]. Unlike flat clustering methods such as k-means [24], hierarchical clustering builds a tree-like structure that reflects nested task similarities. This makes it especially useful in **MTL** settings where task relationships are often complex and nonuniform.

While clustering focuses on grouping tasks to exploit shared structures in **MTL**, another widely used approach in supervised learning is Gradient Boosting (**GB**) [25]. **GB** is an ensemble learning approach that has become one of the most prominent methods in supervised learning, particularly for tabular datasets [26, 27]. Its high performance has inspired the development of several successful derivatives, including XGBoost [28], Light Gradient-Boosting Machine (**LGBM**) [29], and CatBoost [30]. Only a limited number of studies have

investigated extending **GB** to **MTL**, enabling the model to capture both shared and task-specific patterns simultaneously [31, 32]. A more robust variant addresses task diversity by clustering tasks, optimizing model parameters within each cluster, and softly weighting task-cluster assignments using a sigmoid function [33].

A central challenge in ensemble-based **MTL** is task heterogeneity, where tasks differ substantially in input distributions, noise levels, or output structures. When heterogeneous or outlier tasks are forced into joint training, they can distort shared representations and degrade overall performance [34, 6]. As a result, existing ensemble-based extensions to **MTL** often lack robustness to such heterogeneity. For example, Multi-Task Gradient Boosting (**MTGB**) extends **GB** to the **MTL** setting by decomposing each task into shared and task-specific components [32]. However, because all tasks contribute equally to learning the shared structure, **MTGB** remains sensitive to outlier tasks that deviate strongly from the majority, which can negatively influence the ensemble [33]. To address this limitation, a robust extension, Robust-Multi-Task Gradient Boosting (**R-MTGB**), was proposed in [33]. It incorporates a learnable inlier-outlier mechanism that assigns extreme weights to anomalous tasks. Although effective at mitigating the impact of severe outliers, **R-MTGB** relies on a binary assumption in which tasks are categorized strictly as either inliers or outliers, with robustness achieved through this twofold separation. This assumption is restrictive in settings where tasks naturally form multiple heterogeneous groups. More broadly, although **GB** has been extended to **MTL**, existing approaches do not perform task clustering in the sense of **CMTL**. Consequently, the integration of clustering-based **MTL** with boosting (capable of modeling multiple task groups) remains largely unexplored.

To address these challenges, we introduce Robust Multi-Task Boosting using Clustering and Local Ensembling (**RMB-CLE**), a robust **MTL** framework grounded in error-based task relatedness. Rather than relying on in-domain performance or heuristic similarities, **RMB-CLE** estimates functional task similarity through cross-task generalization errors, which provide a principled basis for transferability and cross-task risk. These error-driven representations define a similarity geometry over tasks, from which latent task groups are discovered via hierarchical agglomerative clustering with automatic model selection. Learning then proceeds through cluster-wise local ensembling, enabling selective information sharing within functionally coherent task groups. By jointly integrating error-driven similarity estimation, adaptive task clustering, and localized ensemble learning, **RMB-CLE** structurally mitigates negative transfer under task heterogeneity, going beyond ad-hoc clustering-boosting combinations.

The main contributions of this work are:

- **A principled framework for robust multi-task learning:** We introduce **RMB-CLE**, which infers task relatedness from cross-task generalization errors, providing a theoretically grounded measure of functional similarity that reflects transferability rather than task difficulty.
- **Error-driven discovery of latent task structure:** By embedding tasks in an error-triggered similarity space and applying adaptive hierarchical clustering, **RMB-CLE** automatically uncovers heterogeneous task groups without metadata, predefined partitions, or low-rank assumptions.
- **Mitigation of negative transfer via local ensembling:** Learning is performed through cluster-wise ensemble models that enable selective information sharing within coherent task groups while isolating incompatible tasks, resulting in robustness under distributional shift and task heterogeneity.
- **Extensive empirical validation:** Experiments on synthetic and real-world benchmarks demonstrate that **RMB-CLE** accurately recovers latent task clusters and consistently outperforms single-task, pooling-based, and existing multi-task boosting methods.

The remainder of this paper is organized as follows. Section 2 reviews related work. Section 3 presents the proposed methodology, including the mathematical framework and theoretical motivation. Section 4 describes the experimental setup and reports the results. Section 5 concludes with the main findings. Additional ablation studies and supplementary experimental results are provided in A and B.

## 2 Related work

One of the earliest studies on clustering in **MTL** proposed grouping tasks based on similarity to limit the influence of outliers [11]. The approach relies on a weighted nearest-neighbor framework with Euclidean distances to compute a task transfer matrix that quantifies pairwise relatedness. Another similar study proposed an **MTL** approach that incorporates task clustering to enhance the Bayesian learning process [12]. In this framework, neural networks serve as the base estimators, where the input-to-hidden weights are shared across all tasks, while the hidden-to-output weights are Task-Specific (**TS**). The **TS** parameters

are assumed to be drawn from a Gaussian prior, and the shared parameters are learned empirically using maximum likelihood estimation (empirical Bayes) over all tasks. A Bayesian nonparametric framework for **MTL** was introduced later by [13], employing Dirichlet Process priors to automatically cluster related tasks. The framework supports both Symmetric MTL (SMTL), which performs joint learning, and Asymmetric MTL (AMTL), which enables knowledge transfer without access to the original data. Logistic regression parameters are drawn from a Dirichlet Process-based prior. Variational Bayesian inference is applied in SMTL, and the resulting SMTL posterior is used as a prior in AMTL.

Subsequent research introduced convex and subspace-based formulations for clustering tasks, beginning with the cluster norm of a regularization that balances within-cluster compactness and between-cluster separation, encouraging **TS** weight vectors to form a small number of clusters [35]. Learning the shared subspace for multi-task clustering is proposed in [36], assuming that despite distributional differences, tasks align in a latent space. The model jointly clusters within tasks and across tasks, balanced by a regularization parameter, and optimizes assignments and the projection matrix via alternating minimization with convergence guarantees. A similar study addresses task heterogeneity by aligning distributions across tasks while preserving within-task structure [37]. Using Kernel Hilbert Space with Kernel Mean Matching for alignment and Graph Regularization with Laplacian constraints for structure, kernel k-means in the learned space integrates both sources of information for effective transfer. Later, a unified theoretical framework was proposed in [38], showing the equivalence of Alternating Structure Optimization, which assumes a common low-dimensional feature space, and **CMTL**, which assumes clustered tasks with shared features. Both are reformulated as equivalent optimization problems through spectral relaxation. In addition, a convex relaxation of the non-convex **CMTL** problem is introduced to improve computational efficiency in high-dimensional settings.

Later methods leveraged kernel learning and spectral techniques for cross-task clustering. A learning-based formulation was introduced, combining multi-task feature learning with multiclass maximum-margin clustering [39]. Building on this, multi-task spectral clustering was developed to exploit inter-task correlations through a shared low-dimensional representation with  $\ell_{2,p}$ -norm regularization, while also preserving intra-task structure, enabling both cluster label learning and mapping for out-of-sample data [40]. In a related line of work, the Self-Adapted Multi-Task Clustering model enhances cross-task clustering while reducing negative transfer by selectively reusing instances, using divergence- and kernel-based similarity within a spectral clustering framework to adapt dynamically to task relatedness [41]. Flexible-**CMTL** incorporates instance-based learning by introducing representative tasks as reference points for organizing task relationships, where each task connects to multiple representatives with different weights, allowing flexible soft clustering and adaptive information sharing; the number of clusters is inferred automatically from the data [19]. In addition, a model-based clustering approach performs within-task clustering via symmetric non-negative matrix factorization with linear regression and learns cross-task relatedness by estimating similarities of regression weights to enable knowledge transfer, with an alternating optimization algorithm handling non-convexity [42].

A closely related line of work in deep **MTL** addresses negative transfer by manipulating task gradients during optimization rather than relying on static or heuristic loss weighting. Early work in this direction formulates **MTL** as a multi-objective optimization problem, where the goal is to identify Pareto-stationary solutions that balance competing task objectives instead of minimizing a weighted sum of losses, leading to gradient-based procedures that compute a common descent direction for all tasks and scalable approximations suitable for Deep Neural Network (**DNN**) [43]. Building on this perspective, subsequent methods focus on resolving gradient conflicts directly at each optimization step: one approach modifies task gradients through projection whenever their directions conflict, effectively removing components that would harm progress on other tasks while remaining model-agnostic and compatible with standard optimizers [44]. More recent work further refines gradient-based aggregation by introducing constrained optimization formulations that control the trade-off between improving average task performance and protecting the worst-performing tasks, resulting in more balanced solutions along the Pareto frontier in deep **MTL** [45].

A complementary line of work addresses negative transfer in **MTL** by reasoning about relationships between tasks, rather than modifying optimization dynamics. In the context of transfer learning, Taskonomy studies task relatedness by measuring how representations learned for one task transfer to another, yielding a directed task graph that guides supervision and transfer decisions [46]. However, subsequent work has shown that transfer affinity does not necessarily predict whether tasks should be learned jointly in a multi-task setting, as multi-task compatibility depends strongly on factors such as model capacity, dataset size, and optimization interactions [47].

A recent line of research has extended boosting methods to **MTL** setting. In particular, a two-phase framework known as **MTGB** has been proposed to combine shared and task-specific learning within boosting [32].

In the shared learning phase, **MTGB** fits common base learners across all tasks to extract representations that capture global structure. In the second phase (task-specific learning), it augments these shared representations with **TS** learners trained on the corresponding pseudo-residuals, thereby developing the model to individual tasks. This design allows **MTGB** to balance knowledge transfer with specialization. Despite these advantages, **MTGB** assumes that all tasks should contribute uniformly to the global representation, making it vulnerable to negative transfer in the presence of heterogeneous or noisy tasks [33]. Its extension, **R-MTGB**, addresses this issue by adding an intermediate block that introduces a learnable sigmoid-based weighting scheme [33]. This mechanism softly partitions tasks into outliers and non-outliers, down-weighting adversarial ones before proceeding to task-specific fine-tuning. While **R-MTGB** improves robustness, its binary partitioning restricts flexibility: it can only distinguish between two groups of tasks, ignoring more complex cluster structures.

## 2.1 Comparative analysis

Our proposed **RMB-CLE** framework advances **CMTL** by utilizing a principled, unsupervised agglomerative clustering method to discover latent task relationships through the alignment of cross-task errors. Unlike conventional **CMTL** methods that rely on predefined clusters or low-rank projections, Bayesian nonparametric models [13] requiring complex inference, convex regularization approaches such as cluster norm [35], or subspace learning methods [36, 37] assuming global alignment, **RMB-CLE** derives similarity directly from error-based inter-task behavior, leveraging task-specific local ensembles to remain robust to distributional shifts and heterogeneity. In contrast to spectral clustering [40], or early transfer approaches [11], **RMB-CLE** leverages cross-task error signals to construct adaptive cluster-level ensembles. It remains model-agnostic and avoids reliance on metadata, handcrafted similarity measures, or nearest-neighbor assumptions.

In contrast to gradient-based deep **MTL** methods, which mitigate negative transfer by adjusting gradients within a shared parameterization [43, 44, 45], **RMB-CLE** operates at the level of task relationships. Gradient-based approaches assume that all tasks remain coupled throughout training and address incompatibilities only through local, synchronous optimization corrections. As a result, they neither uncover latent task clusters nor enforce structural separation between incompatible tasks. **RMB-CLE** instead infers functional similarity from cross-task generalization errors and partitions tasks into clusters, preventing negative transfer by isolating unrelated tasks rather than attenuating gradient interference within a shared model.

Complementary to representation-based transfer analyses [46], and model-dependent task grouping strategies [47], our approach defines task similarity directly through cross-task predictive performance and leverages this structure for robust clustered learning. This formulation is model-agnostic, applies beyond deep neural networks, and directly targets the reduction of negative transfer in heterogeneous multi-task settings.

Compared to recent boosting-based approaches such as **MTGB** [32] and its robust extension **R-MTGB** [33], our proposed approach removes the assumption of a fixed or binary partition of tasks. These limitations highlight the need for a more general approach that can adaptively discover multiple task clusters, safeguard against negative transfer without relying on hard or binary partitions, and still preserve task-specific specialization.

Table 1 summarizes the key methodological distinctions among representative **MTL** approaches. In particular, it highlights that gradient-based deep **MTL** methods mitigate negative transfer through optimization-level interventions within a fully shared model, without modeling task structure. Boosting-based multi-task methods therefore form the most relevant comparison class for **RMB-CLE**. Beyond their empirical effectiveness on tabular data [27], they share the ensemble-based learning paradigm underlying **RMB-CLE** and enable controlled information sharing without relying on shared deep representations. Within this class, existing approaches such as **MTGB** and **R-MTGB** enhance robustness via staged boosting or outlier-aware weighting, but remain restricted to global or binary cluster structures and do not support adaptive multi-cluster discovery or cluster-level ensembling.

## 3 Methodology

In this work, **RMB-CLE** is proposed as a framework for identifying and clustering related tasks and training local ensembles within each cluster, enabling knowledge sharing while isolating unrelated tasks to mitigate negative transfer. This section first introduces the necessary preliminaries (Subsection 3.1), then presents

Table 1: Comparison of representative multi-task learning methods. **Grad**: gradient manipulation; **Clust**: discovers task clusters; **Ens**: uses cluster-level ensembles; **Meta**: requires metadata; **Agn**: model-agnostic. (Symbols:  $\checkmark$ =present;  $\times$ =absent).

Method	Grad	Clust	Ens	Meta	Agn
Bayesian-MTL [13]	$\times$	$\checkmark$	$\times$	$\times$	$\times$
Cluster norm [35]	$\times$	$\checkmark$	$\times$	$\times$	$\times$
Shared subspace MTL [36, 37]	$\times$	$\times$	$\times$	$\times$	$\times$
Spectral task clustering [40]	$\times$	$\checkmark$	$\times$	$\times$	$\times$
Gradient-based deep MTL [43]	$\checkmark$	$\times$	$\times$	$\times$	$\checkmark$
Gradient surgery [44]	$\checkmark$	$\times$	$\times$	$\times$	$\checkmark$
Conflict-averse gradients [45]	$\checkmark$	$\times$	$\times$	$\times$	$\checkmark$
MTGB [32]	$\times$	$\times$	$\times$	$\times$	$\checkmark$
R-MTGB [33]	$\times$	$\checkmark$	$\times$	$\times$	$\checkmark$
RMB-CLE (ours)	$\times$	$\checkmark$	$\checkmark$	$\times$	$\checkmark$

the mathematical formulation and algorithmic details of the framework (Subsection 3.2), and finally provides its theoretical justification (Subsection 3.3).

### 3.1 Preliminaries

Let  $\mathcal{T} = \{1, \dots, m\}$  denote the set of supervised tasks. Each task  $i \in \mathcal{T}$  is associated with a labeled dataset  $\mathcal{D}_i = \{(\mathbf{x}_{i,v}, y_{i,v})\}_{v=1}^{n_i}$ , where  $\mathbf{x}_{i,v} \in \mathbb{R}^d$  are input features and  $y_{i,v} \in \mathcal{Y}$  denotes the corresponding supervised target.

For each task  $i$ , we first fit a predictor  $F_i$  via empirical risk minimization,

$$F_i = \underset{F \in \mathcal{H}}{\operatorname{argmin}} \frac{1}{n_i} \sum_{v=1}^{n_i} \ell(y_{i,v}, F(\mathbf{x}_{i,v})), \quad (1)$$

where  $\ell$  is the task-appropriate loss and  $\mathcal{H}$  denotes a hypothesis space of predictive functions. For classification tasks,  $\ell$  is given by the cross-entropy loss,

$$\ell(y_{i,v}, F_i) = - \sum_{q=1}^Q y_{i,q} \ln(P_q), \quad (2)$$

where  $Q$  denotes the number of class labels,  $y_{i,q} \in \{0, 1\}$  is the  $q$ -th component of the one-hot encoded target vector, and  $P_{i,q}$  is the predicted probability associated with class  $q$ , given by  $P_{i,q} = \exp(F_{i,q}) / \sum_{q=1}^Q \exp(F_{i,q})$ . For regression tasks, we instead use the squared error loss,

$$\ell(y_{i,v}, F_i) = \frac{1}{2} (y_{i,v} - F_i)^2. \quad (3)$$

In practice, we instantiate  $\mathcal{H}$  as the class of **LGBM** [29] ensembles ( $\mathcal{H}_{\text{LGBM}}$ ), using decision tree regressor with maximum depth of one (decision stumps) ( $h_{i,t}$ ), trained iteratively with learning rate  $\nu \in (0, 1]$ ,

$$F_{i,t}(\mathbf{x}) = F_{i,(t-1)}(\mathbf{x}) + \nu h_{i,t}(\mathbf{x}), \quad (4)$$

where  $t = 1, \dots, T$  indexes the boosting iterations and  $T$  denotes the total number of boosting rounds. In the remainder of this section, we denote by  $F_i$  the final boosted predictor obtained after  $T$  boosting iterations, i.e.,  $F_i \equiv F_{i,T}$ .

We also introduce the notion of a boosting block. A boosting block  $\mathcal{S}_{(.)}$  denotes a structural unit composed of a fixed number of sequential boosting iterations (i.e., base learners) trained under a specific functional role. Different stages may serve different purposes within a model, such as learning shared representations ( $\mathcal{S}_{(1)}$ ), task-specific components ( $\mathcal{S}_{(2)}$ ), outlier-aware weighting ( $\mathcal{S}_{(3)}$ ), or cluster-level ensembles ( $\mathcal{S}_{(4)}$ ). Accordingly, the size of each block, denoted by  $\mathcal{K}_{\mathcal{S}_{(.)}}$ , may vary across blocks depending on their role in the model.

### 3.2 Framework formulation

**Step 1: Cross-Task Similarity Estimation** To calculate task similarity, we first quantify how well model  $F_j$  (trained on task  $j$ ) transfers to task  $i$  by evaluating it on  $\mathcal{D}_i$ ,

$$E_{i,j} = \begin{cases} \frac{1}{n_i} \sum_{v=1}^{n_i} (y_{i,v} - F_j(\mathbf{x}_{i,v}))^2, & \text{Regression,} \\ 1 - \frac{1}{n_i} \sum_{v=1}^{n_i} \mathbf{1}\{F_j(\mathbf{x}_{i,v}) = y_{i,v}\}, & \text{Classification,} \end{cases} \quad (5)$$

where,  $\mathbf{1}\{\cdot\}$  is the indicator function.

**Remark.** Note that cross-task evaluation is essential, since in-domain accuracy only reflects task difficulty (e.g., noise level or sample size) and not inter-task compatibility. Two unrelated tasks may both be *easy* (low in-domain error) but transfer poorly, while two *hard* tasks may transfer well if their conditional mechanisms are similar. By measuring transferability between tasks, we avoid negative knowledge transfer (see Subsection 3.3) and obtain a principled similarity structure. As a potential alternative, one could consider an out-of-sample cross-task error approach, which we discuss and contrast in A.1.

We then convert the errors to similarities, where smaller cross-task error indicates greater closeness,

$$\mathbf{s}_{i,j} = \frac{1}{E_{i,j} + \varepsilon}, \quad \varepsilon > 0. \quad (6)$$

Collecting these entries across all task pairs returns the similarity matrix,

$$\mathbf{S} = (\mathbf{s}_{i,j})_{i,j=1}^m \in \mathbb{R}^{m \times m}. \quad (7)$$

Thus, each vector  $\mathbf{s}_i = (s_{i,1}, \dots, s_{i,m})$  array can be viewed as a *similarity profile* of task  $i$  relative to all other tasks. In this sense, every task is embedded as a vector in  $\mathbb{R}^m$ , and tasks with similar predictive behavior correspond to similarity vectors that are close in angle. This motivates the use of cosine distance,

$$\Delta_{i,j} = 1 - \frac{\langle \mathbf{s}_i, \mathbf{s}_j \rangle}{\|\mathbf{s}_i\|_2 \|\mathbf{s}_j\|_2}, \quad \Delta_{i,j} \in [0, 1]. \quad (8)$$

**Step 2: Task clustering** For clustering, we define the average linkage distance between two multi-task clusters  $A$  and  $B$ ,

$$\delta(A, B) = \frac{1}{|A||B|} \sum_{i \in A} \sum_{j \in B} \Delta_{i,j}. \quad (9)$$

Applying agglomerative clustering with average linkage (also known as Unweighted Pair Group Method with Arithmetic mean (UPGMA)) [48] on  $\Delta$  produces a dendrogram  $\mathcal{L}$  with  $m$  leaves. For each  $k \in \{2, \dots, \min(m, K_{\max})\}$ , we obtain a partition (assignment function for a given  $k$ )  $g_k : \{1, \dots, m\} \rightarrow \{1, \dots, k\}$  with clusters  $\mathcal{C}_c = \{i : g_k(i) = c\}$ .

**Step 3: Optimal Cluster Search** To choose the best number of clusters, we evaluate the silhouette score [49],

$$\varphi(i) = \frac{b(i) - a(i)}{\max\{a(i), b(i)\}}, \quad (10)$$

where  $a(i) = \frac{1}{|C_{g_k(i)}|-1} \sum_{j \in C_{g_k(i)} \setminus \{i\}} \Delta_{i,j}$  is the inner-cluster distance, and  $b(i) = \min_{c \neq g_k(i)} \frac{1}{|\mathcal{C}_c|} \sum_{j \in \mathcal{C}_c} \Delta_{i,j}$  is the nearest other-cluster distance. Hence the optimal cluster count is,

$$k^* = \operatorname{argmax}_k \frac{1}{m} \sum_{i=1}^m \varphi(i), \quad (11)$$

and the final assignment will be computed as  $g(i) = g_{k^*}(i)$ .

**Step 4: Agglomerative update** Using the Lance and Williams recurrence [50], when clusters  $A$  and  $B$  merge, their distance ( $\delta$ ) to any other cluster  $C$  is updated as,

$$\begin{aligned}\delta(A \cup B, C) &= \alpha_A \delta(A, C) + \alpha_B \delta(B, C) \\ &\quad + \beta \delta(A, B) + \gamma |\delta(A, C) - \delta(B, C)|.\end{aligned}$$

For average linkage (UPGMA), the parameters are given by  $\alpha_A = \frac{|A|}{|A|+|B|}$ ,  $\alpha_B = \frac{|B|}{|A|+|B|}$ , and  $\beta = \gamma = 0$ . The distance update rule is,

$$\delta(A \cup B, C) = \frac{|A| \delta(A, C) + |B| \delta(B, C)}{|A| + |B|}, \quad (12)$$

which ensures that after each merge, cluster-to-cluster distances are updated consistently, enabling the construction of the full dendrogram  $\mathcal{L}$ .

**Step 5: Cluster-specific models** Finally, for each cluster  $c$ , we pool data  $\mathcal{U}_c = \bigcup_{i \in C_c} \mathcal{D}_i$  and train a specialized local ensemble  $f$ ,

$$f_c = \operatorname{argmin}_{f \in \mathcal{F}} \frac{1}{|\mathcal{U}_c|} \sum_{(\mathbf{x}, y, i) \in \mathcal{U}_c} \ell(y, f([\mathbf{x}; i])), \quad (13)$$

where  $\ell$  is the loss function, defined as the cross-entropy loss (Eq. (2)) for classification tasks and the squared error loss (Eq. (3)) for regression tasks. In this study we instantiate  $\mathcal{F}$  with [LGBM](#) [29], which introduces histogram-based feature binning and leaf-wise (Best-first) tree growth for fast, memory-efficient boosting with depth equal to one (decision stumps) and [MTGB](#) [32], which first learns a shared latent function across tasks to capture common structure and then task-specific functions to model individual particularities, both using decision stumps as base learners. Other local [ML](#) models are also compatible.

**Prediction** At prediction time, each input instance comes with a task identifier  $i \in \mathcal{T}$ . Since cluster assignments were already determined during training, prediction reduces to a cluster lookup followed by cluster-specific inference,

$$c = g(i), \quad \hat{y} = f_c([\mathbf{x}; i]), \quad (14)$$

where  $\hat{y}$  is the predicted output for input  $\mathbf{x}$  under task  $i$ ,  $g : \mathcal{T} \rightarrow \{1, \dots, k^*\}$  is the final task-to-cluster assignment and  $f_c$  is the local ensemble trained on  $c$ .

For clarity, we detail the algorithmic structure of [RMB-CLE](#) and provide its pseudocode in Algorithm 1.

### 3.3 Theoretical motivation

This section justifies why cross-task evaluation (Eq. (5)) provides a principled measure of task similarity, whereas evaluating each model only on its own dataset does not.

The key theoretical insight underlying [RMB-CLE](#) is that cross-task generalization error provides a principled basis for task compatibility. In both regression and classification settings, the risk arising when transferring a model across tasks decomposes into a task-dependent noise term and a functional mismatch term that reflects differences between the underlying conditional mechanisms. Consequently, cross-task errors capture functional relatedness rather than task difficulty or noise alone.

By clustering tasks based on this decomposition, [RMB-CLE](#) avoids forcing information sharing between incompatible tasks. Tasks that exhibit large functional mismatch are separated into different clusters, while tasks with compatible conditional mechanisms are grouped together, enabling selective knowledge sharing. This provides a safeguard against negative multi-task transfer.

We formalize this argument in two settings. The regression analysis in Subsection 3.3.1 shows that cross-task risk admits an exact decomposition into a functional distance term and an irreducible noise term. The classification analysis in Subsection 3.3.2 establishes that cross-task error upper-bounds the excess risk in terms of disagreement with the Bayes classifier.

#### 3.3.1 Regression setting

Let task  $i$  be associated with joint distribution  $P_i(X, Y)$ , where  $X \in \mathcal{X}$  denotes inputs and  $Y \in \mathbb{R}$  the output. The regression function is defined as,

$$\eta_i(x) = \mathbb{E}[Y | X = \mathbf{x}, i], \quad (15)$$

---

**Algorithm 1** RMB-CLE Training Algorithm

---

**Require:**  $\{\mathcal{D}_i\}_{i=1}^m, \varepsilon > 0$ , local ensemble  $f \in \mathcal{F}$

- 1: **Apply LGBM:**
- 2: **for**  $i = 1..m$  **do**  $F_i \leftarrow \text{TrainLGBM}(\mathcal{D}_i)$
- 3: **end for**
- 4: **Cross-task errors & similarities:**
- 5: **for**  $i = 1..m$  **do**
- 6:   **for**  $j = 1..m$  **do**
- 7:      $E_{i,j} \leftarrow \text{Eq. (5)}$ ;    $s_{i,j} \leftarrow 1/(E_{i,j} + \varepsilon)$
- 8:   **end for**
- 9: **end for**
- 10: **Cosine distances on similarity arrays:**
- 11: **for**  $i, j = 1..m$  **do**
- 12:    $\Delta_{i,j} \leftarrow \begin{cases} 0, & i = j \\ 1 - \frac{\langle \mathbf{s}_i, \mathbf{s}_j \rangle}{\|\mathbf{s}_i\|_2 \|\mathbf{s}_j\|_2}, & i \neq j \end{cases}$
- 13: **end for**
- 14:  $\Delta \leftarrow \frac{1}{2}(\Delta + \Delta^\top)$
- 15: **Agglomerative clustering (UPGMA):**
- 16:  $Z \leftarrow \text{linkage}(\text{squareform}(\Delta))$
- 17: **for**  $k = 2.. \min(m, K_{\max})$  **do**
- 18:    $g_k \leftarrow \text{fcluster}(Z)$
- 19:   **Silhouette at  $k$ :**
- 20:   **for**  $i = 1..m$  **do**
- 21:      $A \leftarrow \{j : g_k(j) = g_k(i)\}$
- 22:      $a(i) \leftarrow \begin{cases} 0, & |A| = 1 \\ \frac{1}{|A|-1} \sum_{j \in A \setminus \{i\}} \Delta_{i,j}, & \text{else} \end{cases}$
- 23:      $b(i) \leftarrow \min_{c \neq g_k(i)} \frac{1}{|\mathcal{C}_c|} \sum_{j \in \mathcal{C}_c} \Delta_{i,j}$  where  $\mathcal{C}_c = \{j : g_k(j) = c\}$
- 24:      $k^* \leftarrow \text{argmax}_k \varphi_k(i)$  Eq. (10)
- 25:   **end for**
- 26:    $\bar{\varphi}(k) \leftarrow \frac{1}{m} \sum_{i=1}^m \varphi_k(i)$
- 27: **end for**
- 28:  $k^* \leftarrow \arg \max_k \bar{\varphi}(k)$ ;    $g(i) \leftarrow g_{k^*}(i)$ ;    $\mathcal{C} \leftarrow \{i : g(i) = c\}$
- 29: **local ensembles:**
- 30: **for** each  $c$  **do**
- 31:    $\mathcal{U}_c \leftarrow \bigcup_{i \in \mathcal{C}_c} \mathcal{D}_i$ ;    $f_c \leftarrow f_c\{([\mathbf{x}; i], y) : (\mathbf{x}, y, i) \in \mathcal{U}_c\}$
- 32: **end for**
- 33: **return** RMB-CLE-VIA- $\mathcal{F}$

---

that is, the conditional expectation of  $Y$  given  $X = \mathbf{x}$  for task  $i$ . We also define the conditional noise variance as,

$$\sigma_i^2(\mathbf{x}) = \mathbb{E}[(Y - \eta_i(\mathbf{x}))^2 \mid X = \mathbf{x}, i]. \quad (16)$$

Considering  $F_j$  as the predictor trained on task  $j$ . The squared-loss risk of  $F_j$  on task  $i$  is

$$\mathcal{R}_i(F_j) = \mathbb{E}_{P_i}[(Y - F_j(X))^2], \quad (17)$$

where  $P_i$  denotes the joint data-generating distribution of  $(X, Y)$  for task  $i$ .

**Step 1: Conditioning on  $X$**  Using the law of total expectation,

$$\mathcal{R}_i(F_j) = \mathbb{E}_{P_i^X} \left[ \mathbb{E}[(Y - F_j(X))^2 \mid X] \right], \quad (18)$$

where  $P_i^X$  denotes the marginal distribution of the inputs  $X$  under task  $i$ , obtained from the joint distribution  $P_i(X, Y)$ . The inner expectation is taken with respect to the conditional distribution  $P_i^{Y|X}$ , i.e.,  $P_i(Y \mid X)$ .

**Step 2: Expanding inside the conditional expectation** For a fixed  $X = \mathbf{x}$  we write  $Y = \eta_i(\mathbf{x}) + \varepsilon_i$ , where  $\mathbb{E}[\varepsilon_i \mid X = \mathbf{x}] = 0$  and  $\mathbb{E}[\varepsilon_i^2 \mid X = \mathbf{x}] = \sigma_i^2(\mathbf{x})$ . Then,

$$\mathbb{E}[(Y - F_j(x))^2 \mid X = x] = \mathbb{E}[(\eta_i(\mathbf{x}) + \varepsilon_i - F_j(\mathbf{x}))^2 \mid X = \mathbf{x}]. \quad (19)$$

Expanding the square gives,

$$(\eta_i(\mathbf{x}) - F_j(\mathbf{x}))^2 + 2(\eta_i(\mathbf{x}) - F_j(\mathbf{x}))\mathbb{E}[\varepsilon_i | X = x] + \mathbb{E}[\varepsilon_i^2 | X = \mathbf{x}]. \quad (20)$$

The middle term vanishes because  $\mathbb{E}[\varepsilon_i | X = x] = 0$ , hence,

$$\mathbb{E}[(Y - F_j(\mathbf{x}))^2 | X = \mathbf{x}] = (\eta_i(x) - F_j(\mathbf{x}))^2 + \sigma_i^2(\mathbf{x}). \quad (21)$$

**Step 3: Taking expectation over  $X$**  Plugging this back gives,

$$\mathcal{R}_i(F_j) = \mathbb{E}_{P_i^X}[(\eta_i(X) - F_j(X))^2 + \sigma_i^2(X)]. \quad (22)$$

Separating the terms,

$$\mathcal{R}_i(F_j) = \underbrace{\mathbb{E}_{P_i}[(\eta_i(X) - F_j(X))^2]}_{(1)} + \underbrace{\mathbb{E}_{P_i}[\sigma_i^2(X)]}_{(2)}. \quad (23)$$

Thus, the cross-task error decomposes into (1) a task similarity term measuring the squared  $L^2$ -distance between the conditional functions  $\eta_i$  and  $F_j$ , and (2) a noise term that is independent of  $F_j$ .

### 3.3.2 Classification setting

For each task  $i \in \{1, \dots, m\}$ , let  $(X, Y) \sim P_i$ , where  $X \in \mathcal{X}$  denotes the feature vector and  $Y \in \{1, \dots, K\}$  the class label, with  $K \geq 2$ . We write  $\Pr(\cdot)$  for probability with respect to the task-specific distribution  $P_i$ . The class-posterior function for task  $i$  is defined as

$$\eta_i(x) = (\Pr(Y = 1 | X = \mathbf{x}, i), \dots, \Pr(Y = K | X = \mathbf{x}, i)). \quad (24)$$

The corresponding Bayes classifier is

$$b_i(\mathbf{x}) = \operatorname{argmax}_{k \in \{1, \dots, K\}} \Pr(Y = k | X = \mathbf{x}, i). \quad (25)$$

For  $K = 2$ , this reduces to the binary Bayes rule  $b_i(\mathbf{x}) = \mathbf{1}\{\eta_i(\mathbf{x}) \geq \frac{1}{2}\}$ . For any classifier  $F$ , the (0–1) risk on task  $i$  is

$$\mathcal{R}_i(F) = \Pr_{(X, Y) \sim P_i}(F(X) \neq Y). \quad (26)$$

**Step 1: Excess risk vs. disagreement** The additional error of using  $F_j$  (trained on task  $j$ ) instead of  $b_i$  (Bayes on task  $i$ ) satisfies

$$\mathcal{R}_i(F_j) - \mathcal{R}_i(b_i) \leq \Pr_{P_i^X}(F_j(X) \neq b_i(X)). \quad (27)$$

*Justification.* Condition on  $X = \mathbf{x}$ . For a fixed  $\mathbf{x}$ , the conditional 0–1 risk of a classifier  $F$  is  $\Pr(Y \neq F(X) | X = \mathbf{x})$ . The Bayes classifier  $b_i$  minimizes this quantity over all classifiers, hence,

$$\Pr(Y \neq F_j(X) | X = \mathbf{x}) - \Pr(Y \neq b_i(X) | X = \mathbf{x}) \geq 0. \quad (28)$$

Moreover, if  $F_j(\mathbf{x}) = b_i(\mathbf{x})$ , then both classifiers make the same prediction at  $\mathbf{x}$  and therefore have identical conditional risk, implying that the difference is zero. If  $F_j(\mathbf{x}) \neq b_i(\mathbf{x})$ , then the difference in conditional risks is at most 1, since probabilities are bounded by  $[0, 1]$ . Combining both cases returns

$$\Pr(Y \neq F_j(X) | X = \mathbf{x}) - \Pr(Y \neq b_i(X) | X = \mathbf{x}) \leq \mathbf{1}\{F_j(\mathbf{x}) \neq b_i(\mathbf{x})\}. \quad (29)$$

Taking expectation with respect to  $X \sim P_i^X$  on both sides and using the law of total expectation,

$$\begin{aligned} \mathcal{R}_i(F_j) - \mathcal{R}_i(b_i) &= \mathbb{E}_{X \sim P_i^X} [\Pr(Y \neq F_j(X) | X) - \Pr(Y \neq b_i(X) | X)] \\ &\leq \mathbb{E}_{X \sim P_i^X} [\mathbf{1}\{F_j(X) \neq b_i(X)\}] \\ &= \Pr_{P_i^X}(F_j(X) \neq b_i(X)). \end{aligned} \quad (30)$$

**Step 2: Cross-task error as a similarity measure** The bound in Step 1 shows that transferring a model  $F_j$  to task  $i$  leads to excess error controlled by the probability of disagreement with the Bayes classifier of task  $i$ . When  $F_j$  is a statistically consistent approximation of the latent Bayes rule  $b_j$ , this disagreement reflects a functional mismatch between the class-posterior distributions  $\eta_i$  and  $\eta_j$ . Therefore, the empirical cross-task error  $E_{i,j}$  in Eq. (5) serves as a practical basis for inter-task compatibility in classification.

To further strengthen the theoretical analysis, we examine the computational costs of both the proposed and existing models with respect to training and latency, as detailed in B.1. While the B.1 shows that the proposed model has higher training complexity (due to cross-task evaluation and clustering), its prediction is comparable to or lower than that of the studied models. This efficiency arises because predictions rely solely on the relevant cluster ensemble, making the model more time-efficient at test time compared to state-of-the-art multi-task boosting approaches.

## 4 Experiments and results

The proposed approach is evaluated on both synthetic and real-world datasets to assess performance, robustness, and generalization, and is compared against state-of-the-art Single-Task (ST) and Multi-Task (MT) baselines. Subsection 4.1 introduces the datasets used in the experiments, while Subsection 4.2 describes the experimental setup and the considered baseline methods. Results on synthetic and real-world data are reported in Subsections 4.3 and 4.4, respectively. Ablation experiments and additional analyses are presented in A and B.

### 4.1 Datasets

To precisely evaluate the performance of the proposed framework, and to test the robustness of our approach, we employ a diverse set of datasets comprising both synthetic and real-world MT data.

**Synthetic datasets** We define a generic Random Fourier Feature [51] labeling function,

$$\Upsilon_\psi(\mathbf{x}) = \sqrt{\frac{2\tau}{\kappa}} \sum_{r=1}^{\kappa} \phi_r \cos\left(\frac{1}{\lambda d} \mathbf{w}_r^\top \mathbf{x} + b_r\right), \quad (31)$$

where the parameter set  $\psi = (\phi, \mathbf{W}, \mathbf{b})$  consists of  $\phi = \{\phi_r\}_{r=1}^{\kappa}$ ,  $\mathbf{W} = \{\mathbf{w}_r\}_{r=1}^{\kappa}$  with  $\mathbf{w}_r \stackrel{iid}{\sim} \mathcal{N}(\mathbf{0}, \mathbf{I}_d)$ , and phase shifts  $\mathbf{b} = \{b_r\}_{r=1}^{\kappa}$  with  $b_r \stackrel{iid}{\sim} \mathcal{U}(0, 2\pi)$ . The weights satisfy  $\phi_r \stackrel{iid}{\sim} \mathcal{N}(0, 1)$ . The constants  $\kappa$  and  $d$  denote the number of random features and the input dimension, respectively, while  $\tau$  is a scaling hyperparameter. And  $\lambda > 0$  denotes the length scale.

This construction corresponds to an approximate draw from a Gaussian process [52] with a shift-invariant squared exponential kernel.

Building on this foundation, we generate a set of  $\mathcal{C}$  clusters. Each cluster  $c \in \mathcal{C}$  contains  $m_c$  tasks indexed by  $i \in \{1, \dots, m_c\}$ . For each task  $i$ , we define a synthetic labeling function as the aggregation of a common component (CC) and a task-specific (TS) component. Specifically, we instantiate two independent Random Fourier Feature functions from (31),

$$\Upsilon_c^{\text{CC}}(\mathbf{x}) \equiv \Upsilon_{\psi_c^{\text{CC}}}(\mathbf{x}_{i,v}), \quad (32)$$

$$\Upsilon_c^{\text{TS}}(\mathbf{x}) \equiv \Upsilon_{\psi_c^{\text{TS}}}(\mathbf{x}_{i,v}), \quad (33)$$

where  $\psi_c^{\text{CC}}$  and  $\psi_c^{\text{TS}}$  are independently sampled parameter sets. The resulting function values for input  $\mathbf{x}_i$  are then given by

$$v^{\text{CC}} = \Upsilon_c^{\text{CC}}(\mathbf{x}_{i,v}), \quad (34)$$

$$v^{\text{TS}} = \Upsilon_c^{\text{TS}}(\mathbf{x}_{i,v}). \quad (35)$$

Finally, the output for task  $i$  in cluster  $c$  is generated as a convex combination of its common and task-specific components,

$$y_{i,v}(\mathbf{x}_{i,v}) = \omega v^{\text{CC}}(\mathbf{x}_{i,v}) + (1 - \omega) v^{\text{TS}}(\mathbf{x}_{i,v}), \quad (36)$$

where  $\omega \in (0, 1]$  controls the balance between common and task-specific contributions. For regression tasks, Eq. (36) is used directly, while for classification tasks, binary labels are obtained by thresholding Eq. (36) at its task-specific median value, assigning label 1 to samples with  $y_{i,v}$  above the median and 0 otherwise.

Figure 1 provides a visual example of a generated synthetic dataset with  $\mathcal{T} = 8$  tasks in one dimension ( $d = 1$ ), grouped into  $\mathcal{C} = 4$  clusters, where  $\omega = 0.9$  is used. Colors denote clusters, while symbols distinguish tasks. This illustration is provided for visualization purposes only.

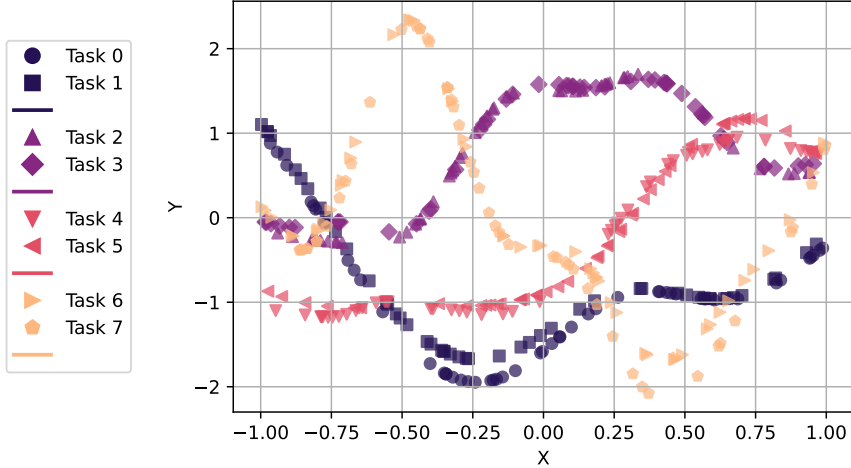


Figure 1: One-dimensional synthetic multi-task dataset with  $\mathcal{T} = 8$ ,  $\mathcal{C} = 4$ , and  $\omega = 0.9$ . Colors indicate clusters and markers denote tasks.

For the experiments, we generate synthetic data using 100 repetitions with different random seeds. Each repetition contains 25 tasks evenly distributed across five clusters, constructed with  $\omega = 0.9$ . Inputs  $\mathbf{x}$  are sampled uniformly from  $[-1, 1]^{d_x}$ , where  $d_x$  is the input dimension. Each task has 300 training samples and 1,000 test samples, with five input features. In regression setting, we use the real-valued outputs from the data-generating process. In classification setting, continuous outputs are first generated and converted into binary labels by thresholding at the task-specific median, computed prior to the train-test split. Samples above the median are labeled 1 and the rest 0. All generated synthetic datasets are publicly available via Mendeley Data<sup>1</sup>.

**Real-world datasets** We also included real-world multi-task datasets, encompassing both classification and regression problems, carefully selected from established multi-task studies [53, 54, 55, 56] across diverse domains, including image recognition [57], finance and insurance [58], healthcare [59, 60], and marketing [61]. These datasets present a variety of challenges, including differences in the number of tasks, instances, and labels, as well as varying degrees of task-relatedness. In each dataset, tasks are obtained by grouping samples according to specific attribute values (e.g., demographic categories or organizational units). Additional complexities arise from class imbalances, skewed label distributions, and the presence of noise and outliers. Table 2 summarizes the real-world multi-task datasets along with their corresponding references. Notably, the *Avila* dataset contains 12 class labels, while the other classification datasets are binary. For the *Adult* dataset, tasks are defined by dividing the population into gender and race categories, resulting in two separate datasets: *Adult-Gender* and *Adult-Race*.

## 4.2 Setup

Experiments were implemented in Python using open-source libraries. The **RMB-CLE** implementation, synthetic data generators, and datasets are publicly available<sup>2</sup> to ensure reproducibility. All runs were executed on a standard multi-core CPU server with 48 GB RAM.

Regarding the baseline methods, we benchmarked **RMB-CLE** against several state-of-the-art boosting methods, a natural comparison since our approach also employs boosting as the local ensemble with supervised ensembling. This choice is further motivated by the fact that ensemble methods based on decision trees consistently achieve state-of-the-art performance on tabular data, particularly in settings similar to those considered here, often outperforming deep learning alternatives [27]. Other approaches discussed in Section 2, such as deep **MTL** methods based on shared representations and gradient-level optimization (e.g.,

<sup>1</sup>[data.mendeley.com/datasets/3gms2fv93/](http://data.mendeley.com/datasets/3gms2fv93/)

<sup>2</sup>[github.com/GAA-UAM/RMB-CLE](http://github.com/GAA-UAM/RMB-CLE)

Table 2: Real-world multi-task datasets description.

Name	Instances	Features	Tasks
<b>Classification</b>			
Avila [62]	20,867	10	48
Adult [63]	48,842	14	7
Bank Marketing [58]	45,211	16	12
Landmine [64]	14,820	9	29
<b>Regression</b>			
Abalone [65]	4,177	8	3
Computer [66]	3,800	13	190
Parkinsons [67]	5,875	19	42
SARCOS [68]	342,531	21	7
School [12]	15,362	10	139

multi-objective formulations and gradient conflict resolution techniques [43, 44, 45]), operate through fundamentally different training dynamics and do not discover task clusters. Including them as primary baselines would therefore conflate architectural and optimization differences rather than isolate the effect of error-driven task clustering and local ensembling. For completeness, however, we include a direct empirical comparison with a representative deep multi-task learning model in Subsection 4.3.

The baselines include both **MT** and **ST** variants. Dedicated **MT** models include **MTGB** [32], which consists of two training blocks: the first uses common estimators to capture shared features across tasks ( $\mathcal{S}_{(1)}$ ), while the second includes task-specific estimators to model task-specific patterns ( $\mathcal{S}_{(2)}$ ), and **R-MTGB** [33], which extends **MTGB** by adding an intermediate block ( $\mathcal{S}_{(3)}$ ) to handle outliers using learnable parameters  $\sigma(\theta)$  that assign extreme weights, allowing the model to emphasize or de-emphasize outliers relative to non-outliers as needed. Heuristic **MT** baselines included Data Pooling (**DP**), which merges all tasks into a single dataset and trains one global model and Task-as-Feature (**TaF**), which augments the input of the **DP** approach by concatenating a one-hot encoding of the task index so the model can learn task-specific adjustments. For **ST** comparison, **GB** [25] and **LGBM** [29] were implemented. Also, heuristic **MT** variants were instantiated with **GB** and **LGBM**. Finally, we employed both **MTGB** and **LGBM** as local ensembles in the proposed **RMB-CLE** framework, resulting in two variants: RMB-CLE-via-MTGB and RMB-CLE-via-LGBM. To evaluate the ability of **RMB-CLE** to identify clusters of related tasks, we compared it with *cluster-known* baselines that were given the true task clusters. This comparison is limited to the synthetic experiments and serves as an upper bound for assessing how closely the proposed framework approximates optimal clustering performance.

Regarding the evaluation protocol, datasets have varying numbers of tasks and a large number of experimental repetitions. For each of the 100 repetitions, model performance on unseen data was first averaged across all tasks and instances. We then computed the overall mean and Standard Deviation (**Std Dev**) across repetitions. Each repetition corresponds to a different 80:20 train-test split for real-world datasets or a different generated dataset for synthetic experiments.

To ensure fair comparison across models, hyperparameters were selected using within-training 5-fold cross-validation. Model configurations were chosen to optimize negative Root Mean Squared Error (**RMSE**) for regression and accuracy for classification. To reduce variability from extensive tuning and maintain comparability, the grid search was limited to the number of estimators (i.e., base learners). All other hyperparameters were kept at their default values from the underlying **scikit-learn** implementation<sup>3</sup> [69]. For all ensemble-based models, decision tree regressors were used as base learners with depth of one (i.e., decision stumps) to maintain consistency across methods and limit the influence of individual tree complexity on overall performance. The hyperparameter search space for all boosting-based baselines, as well as for the proposed **RMB-CLE** framework, includes the number of predictors (block size ( $K_{\mathcal{S}_{(.)}}$ )) in each boosting block ( $\mathcal{S}_{(.)}$ ), as defined in Subsection 3.1. The corresponding search space is summarized in Table 3. For **R-MTGB**, three sequential boosting blocks were tuned following the architecture proposed in [33], whereas **MTGB** baseline was tuned using two blocks as in [32]. Pooling-based baselines were tuned using a single global boosting block trained on the pooled data from all tasks. Single-task baselines (e.g., **ST-GB** and

<sup>3</sup>[github.com/scikit-learn](https://github.com/scikit-learn)

Table 3: Hyperparameter search space for studied models.

Method	Boosting block ( $\mathcal{S}_{(.)}$ )	Block size ( $K_{\mathcal{S}_{(.)}}$ )
Single-task approaches	$\mathcal{S}_{(2)}$	{20, 30, 50, 100}
Pooling-based approaches	$\mathcal{S}_{(1)}$	{20, 30, 50, 100}
MTGB	$\mathcal{S}_{(1)}$	{20, 30, 50}
	$\mathcal{S}_{(2)}$	{0, 20, 30, 50, 100}
R-MTGB	$\mathcal{S}_{(1)}$	{0, 20, 30, 50}
	$\mathcal{S}_{(2)}$	{0, 20, 30, 50, 100}
	$\mathcal{S}_{(3)}$	{20, 30, 50}
RMB-CLE-via-LGBM	$\mathcal{S}_{(2)}$	{20, 30, 50, 100}
	$\mathcal{S}_{(4)}$	{100}
RMB-CLE-via-MTGB	$\mathcal{S}_{(1)}$	{20, 30, 50}
	$\mathcal{S}_{(2)}$	{0, 20, 30, 50, 100}
	$\mathcal{S}_{(4)}$	{100}

[ST-LGBM](#)) were tuned independently for each task using a per-task boosting block. For [RMB-CLE](#), the number of base learners in the local ensembles (Eq. (13)) was selected according to the underlying ensemble instantiation: a single shared learning block across all tasks when using [LGBM](#), and two sequential blocks when using [MTGB](#).

For statistical comparison, we perform a task-wise comparison of task-specific models, with each model evaluated on the average performance of each task across all repetitions. Accuracy is used for 96 classification tasks and [RMSE](#) for 381 regression tasks. Rankings in the Dems  r horizontal plots (lower is better) are based on average ranks computed across tasks and compared using the Nemenyi post-hoc test [70]. A statistically significant difference between two models is indicated when they are not connected by a solid black line, meaning their difference in average ranks exceeds the corresponding Critical Distance ([CD](#)). We report average ranks separately for synthetic and real-world benchmarks to distinguish controlled settings with known latent task structure from heterogeneous real data.

### 4.3 Synthetic results

Table 4 summarizes the mean and [Std Dev](#) of the performance of the evaluated models on the multi-task synthetic classification and regression datasets. The top scores are highlighted in **bold**. The results show that RMB-CLE-via-LGBM consistently achieves the highest accuracy ( $\approx 0.901$ ) and the lowest RMSE ( $\approx 0.275$ ). Notably, the [ST](#) baseline, particularly ST-LGBM, outperforms most conventional [MT](#) methods, including [MTGB](#), [R-MTGB](#), and pooling-based strategies. This behavior suggests that these [MT](#) approaches are not robust to task heterogeneity, and that their performance deteriorates in the presence of outlier or weakly related tasks due to negative transfer. In comparison, [RMB-CLE](#) mitigates this issue by identifying and separating heterogeneous task groups prior to knowledge sharing. While [R-MTGB](#) partially improves robustness by distinguishing outlier from non-outlier tasks, it is limited to a binary partition.

Moreover, to further substantiate the trends observed in Table 4, we report complementary evaluation metrics in Table 5. In particular, this table presents macro-averaged classification recall (equal weight across classes) and the regression Mean Absolute Error ([MAE](#)). The best results for each dataset are highlighted in **bold**.

The results indicate that RMB-CLE-via-LGBM achieves the highest macro recall ( $\approx 0.901$ ) and the lowest MAE ( $\approx 0.215$ ), confirming the consistent superiority of the proposed framework when leveraging LGBM. The close correspondence between recall and accuracy values, as observed in Table 4, demonstrates the robustness of the model, indicating that improvements in sensitivity are not achieved at the expense of overall predictive performance. On the other hand, baseline methods exhibit lower recall and significantly higher MAE, emphasizing the stability and effectiveness of the proposed clustering-based multi-task ensembling approach.

Furthermore, in Tables 4 and 5, the oracle *Cluster-Known* baselines, which are given direct access to the ground-truth task clusters and therefore bypass the clustering step, achieve identical performance to the corresponding [RMB-CLE](#) variants. This result indicates that the proposed framework effectively recovers

Table 4: Synthetic multi-task results (mean  $\pm$  Std Dev). Accuracy (classification) and RMSE (regression); Best results in bold.

Model	Accuracy	RMSE
RMB-CLE-via-LGBM	<b>0.900 <math>\pm</math> 0.015</b>	<b>0.278 <math>\pm</math> 0.017</b>
Cluster-Known-LGBM	<b>0.900 <math>\pm</math> 0.015</b>	<b>0.278 <math>\pm</math> 0.017</b>
ST-LGBM	0.789 $\pm$ 0.026	0.450 $\pm$ 0.032
RMB-CLE-via-MTGB	0.767 $\pm$ 0.029	0.550 $\pm$ 0.039
Cluster-Known-MTGB	0.767 $\pm$ 0.029	0.550 $\pm$ 0.039
ST-GB	0.759 $\pm$ 0.028	0.549 $\pm$ 0.038
MTGB	0.698 $\pm$ 0.079	0.783 $\pm$ 0.143
R-MTGB	0.690 $\pm$ 0.074	0.777 $\pm$ 0.102
DP-LGBM	0.616 $\pm$ 0.039	0.840 $\pm$ 0.113
TaF-LGBM	0.616 $\pm$ 0.038	0.791 $\pm$ 0.089
DP-GB	0.611 $\pm$ 0.038	0.841 $\pm$ 0.113
TaF-GB	0.611 $\pm$ 0.038	0.800 $\pm$ 0.090

Table 5: Synthetic multi-task results (mean  $\pm$  Std Dev). Recall (classification) and MAE (regression); Best results in bold.

Model	Recall	MAE
RMB-CLE-via-LGBM	<b>0.901 <math>\pm</math> 0.016</b>	<b>0.218 <math>\pm</math> 0.013</b>
Cluster-Known-LGBM	<b>0.901 <math>\pm</math> 0.016</b>	<b>0.218 <math>\pm</math> 0.013</b>
ST-LGBM	0.789 $\pm$ 0.026	0.351 $\pm$ 0.025
ST-GB	0.759 $\pm$ 0.028	0.434 $\pm$ 0.030
RMB-CLE-via-MTGB	0.767 $\pm$ 0.029	0.435 $\pm$ 0.031
Cluster-Known-MTGB	0.767 $\pm$ 0.029	0.435 $\pm$ 0.031
R-MTGB	0.690 $\pm$ 0.074	0.624 $\pm$ 0.086
MTGB	0.698 $\pm$ 0.079	0.630 $\pm$ 0.121
TaF-LGBM	0.616 $\pm$ 0.038	0.636 $\pm$ 0.076
TaF-GB	0.611 $\pm$ 0.038	0.643 $\pm$ 0.076
DP-LGBM	0.616 $\pm$ 0.039	0.676 $\pm$ 0.093
DP-GB	0.611 $\pm$ 0.038	0.677 $\pm$ 0.093

the true latent task structure from cross-task error information, reaching the same performance as an idealized method with perfect cluster knowledge.

However, conventional [MTL](#) approaches exhibit poor performance, often failing to outperform [ST](#) baselines. As shown in Tables 4 and 5, standard multi-task boosting methods such as [MTGB](#) and [R-MTGB](#) suffer performance degradation when the task landscape comprises multiple heterogeneous clusters, despite modeling shared and task-specific components. Single-task models (e.g., [ST-LGBM](#)) consistently outperform these [MT](#) baselines, indicating that naïve or insufficiently structured information sharing can be more harmful than no sharing at all.

To further analyze performance at the task level, the rankings of the synthetic tasks are shown in Figure 2: classification tasks in the left subplot and regression tasks in the right subplot. The proposed framework achieved performance identical to the upper bound, represented by *Cluster-Known*, for both [MTGB](#) and [LGBM](#) as local ensembles. Moreover, the proposed framework with [LGBM](#) obtained the best ranking, followed by [ST-LGBM](#) and the proposed approach with [MTGB](#), across all problems (all subplots). We observe that the proposed framework with [LGBM](#) is not statistically different from [ST-LGBM](#) in both classification and regression problems. However, it shows statistically significant differences compared to all other models. On the other hand, the conventional boosting-based multi-task models ([R-MTGB](#) and [MTGB](#)) consistently achieved the lowest rankings across all tasks (all subplots).

To complement the boosting-based comparisons presented in the main experiments, we include an additional baseline based on deep [MTL](#) with shared representations. This experiment is intended to assess how a representative neural multi-task model compares to the proposed framework (under the same synthetic dataset generated and used to train and evaluate the studied models), while acknowledging the fundamentally different modeling assumptions.

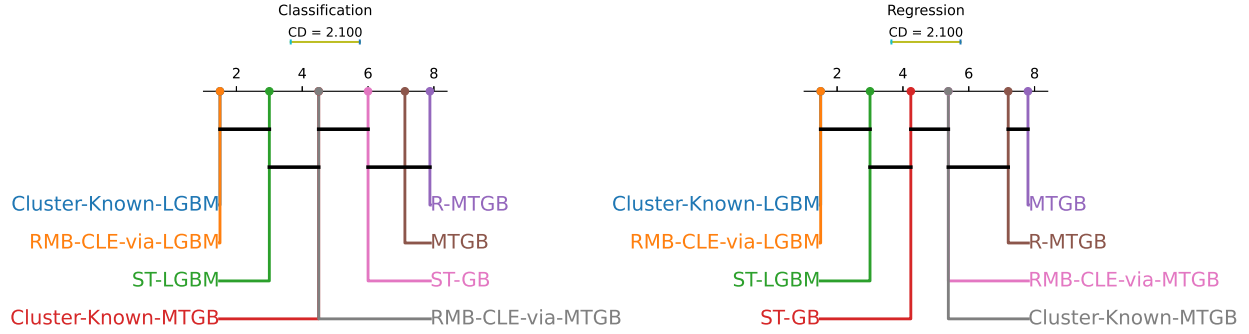


Figure 2: Synthetic task-wise Demšar plots ( $p = 0.05$ ) comparing multi-task models; solid lines indicate no significant differences (Nemenyi).

We adopt a shared neural architecture implemented using `scikit-learn`, consisting of a Multi-Layer Perceptron (MLP) that learns a common feature representation across all tasks (Deep-MTL). The shared network comprises three fully connected hidden layers, each with 100 units and ReLU activation functions. This shared representation is followed by task-specific output heads, with one head per task. For regression problems, each task head is implemented as a ridge regression model, while for classification problems, task heads are implemented as logistic regression classifiers.

The shared MLP is trained on pooled data from all tasks without using task identifiers as input features, thereby enforcing full parameter sharing in the representation layers. Training is performed using the *Adam* optimizer with a learning rate of  $10^{-3}$ , a maximum of 100 iterations, and early stopping enabled. The  $\ell_2$  regularization parameter is fixed to  $10^{-4}$ . After training, the learned hidden representation (defined as the output of the final hidden layer) is extracted and used as input to train task-specific heads independently for each task. For these heads, ridge regression with regularization parameter  $\alpha = 1.0$  is used in regression settings, while logistic regression with inverse regularization strength equal to 1.0 is used for classification. All experiments use the same random seeds, data splits, and evaluation protocol as in previous experiments.

Tables 6 and 7 report the performance of a representative Deep-MTL model based on a shared neural representation. Compared to the boosting-based baselines reported in Tables 4 and 5, Deep-MTL model achieves moderate performance in both classification and regression. While the model benefits from parameter sharing across tasks, its accuracy and recall remain below those of RMB-CLE, and its regression errors (RMSE and MAE) are notably higher.

Table 6: Synthetic multi-task performance of the deep MTL baseline (mean  $\pm$  Std Dev). Accuracy (classification) and RMSE (regression). Results are obtained using the same synthetic data, splits, and evaluation protocol as in Tables 4 and 5.

Model	Accuracy	RMSE
Deep-MTL	$0.848 \pm 0.015$	$0.313 \pm 0.022$

Table 7: Synthetic multi-task performance of the deep MTL baseline (mean  $\pm$  Std Dev). Recall (classification) and MAE (regression). Results are obtained using the same synthetic data, splits, and evaluation protocol as in Tables 4 and 5.

Model	Recall	MAE
Deep-MTL	$0.848 \pm 0.015$	$0.244 \pm 0.017$

To further investigate the robustness of our method, we conducted an additional ablation study (reported in A.2) to evaluate the sensitivity of the clustering stage to the choice of linkage criterion. Average and complete linkage differ in how inter-cluster distances are defined during hierarchical agglomerative clustering: average linkage relies on the mean pairwise distance between tasks across clusters, whereas complete linkage considers the maximum such distance, resulting in more compact clusters [22, 50]. Despite these differences, both strategies yield identical performance (see A.2), indicating that the proposed error-based similarity

Table 8: Ground-truth task-to-cluster assignments in the synthetic data.

Cluster ID	Task indices
0	[0, 1, 2, 3, 4]
1	[5, 6, 7, 8, 9]
2	[10, 11, 12, 13, 14]
3	[15, 16, 17, 18, 19]
4	[20, 21, 22, 23, 24]

representation produces a well-structured and stable task geometry. Consequently, the recovered task groups are robust to the specific rule used for cluster merging.

Moreover, we measured the elapsed runtime of the studied models under three different scenarios on the generated synthetic datasets, with detailed results reported in B.2. The experiments indicate that pooling-based models with **LGBM** are the fastest, whereas multi-task boosting methods (**MTGB**, **R-MTGB**) have substantially higher training times due to their sequential multi-block architectures. Notably, RMB-CLE-via-LGBM matches the *Cluster-Known* baseline in total training time, remaining considerably faster than **MTGB** and **R-MTGB**, while RMB-CLE-via-MTGB exhibits the higher runtime characteristic of multi-task boosting.

#### 4.3.1 Cluster stability analysis

To assess the stability of the inferred task clusters, Figure 3 reports the frequency with which each task is assigned to each cluster over 100 independent runs by the proposed framework. For both regression (top panel) and classification (bottom panel). In each heatmap (panel), columns represent individual tasks and rows correspond to cluster indices. Each cell shows the fraction of runs in which a given task was assigned to a particular cluster, with higher color intensity indicating more frequent assignments. Figure 3 reveals that tasks that belong to the same ground-truth cluster (Table 8) are consistently mapped to the same inferred cluster, with assignment frequencies close to one, while assignments to other clusters remain near zero. This pattern indicates that the clustering procedure is not sensitive to random initialization or data splits and reliably recovers the latent task structure embedded in the synthetic data. Minor dispersion observed in the classification setting reflects the higher stochasticity induced by thresholded labels, yet the dominant cluster memberships remain stable across runs.

Moreover, Table 4 quantitatively confirms this observation, showing that the proposed **RMB-CLE** framework achieves performance identical to the oracle *Cluster-Known* baseline, which has access to the true task-to-cluster assignments. The coincidence of predictive performance implies that the clusters inferred by **RMB-CLE** are effectively equivalent to the ground-truth clusters for the purpose of learning.

To contextualize the clustering behavior of the **R-MTGB** model, we analyze the task-wise behavior of the sigmoid-based weighting mechanism ( $\sigma(\theta_i)$ ) employed in **R-MTGB** across multiple runs. In **R-MTGB**,  $\theta_i$  is a learnable, task-specific scalar parameter that controls the relative contribution of each task to the shared boosting stage by softly gating tasks as either inliers or outliers. Through the sigmoid transformation,

$$\sigma(\theta_i) = \frac{1}{1 + \exp(-\theta_i)},$$

each task is assigned a continuous weight in the interval (0, 1) [33]. Values of  $\sigma(\theta)$  close to 1 indicate tasks that are coupled to the shared representation (inliers), while values close to 0 correspond to tasks that are effectively down-weighted and treated as outliers. Depending on the sign convention of  $\theta_i$ , this interpretation may be reversed, but the underlying behavior remains unchanged. If the underlying task structure aligns with the assumptions of **R-MTGB**, the learned  $\theta$  values are expected to be stable across runs and to concentrate near the extremes. However, when the true task landscape contains multiple coherent clusters, the use of a single scalar parameter  $\theta_i$  per task becomes too limited to capture this structure. In this case,  $\theta$  can only encode a one-dimensional gating decision and is therefore unable to represent richer multi-cluster structure. Consequently, the sigmoid weighting mechanism ( $\sigma(\theta)$ ) is forced to collapse several distinct task groups into an soft binary partition. As a result, and as illustrated in Figure 4, the learned  $\theta$  values exhibit substantial variability across runs and tasks, failing to produce a stable or interpretable task separation.

Figure 4 highlights this limitation by visualizing the learned  $\sigma(\theta)$  values across tasks and runs for both regression (top panel) and classification (bottom panel). In this figure, columns correspond to different

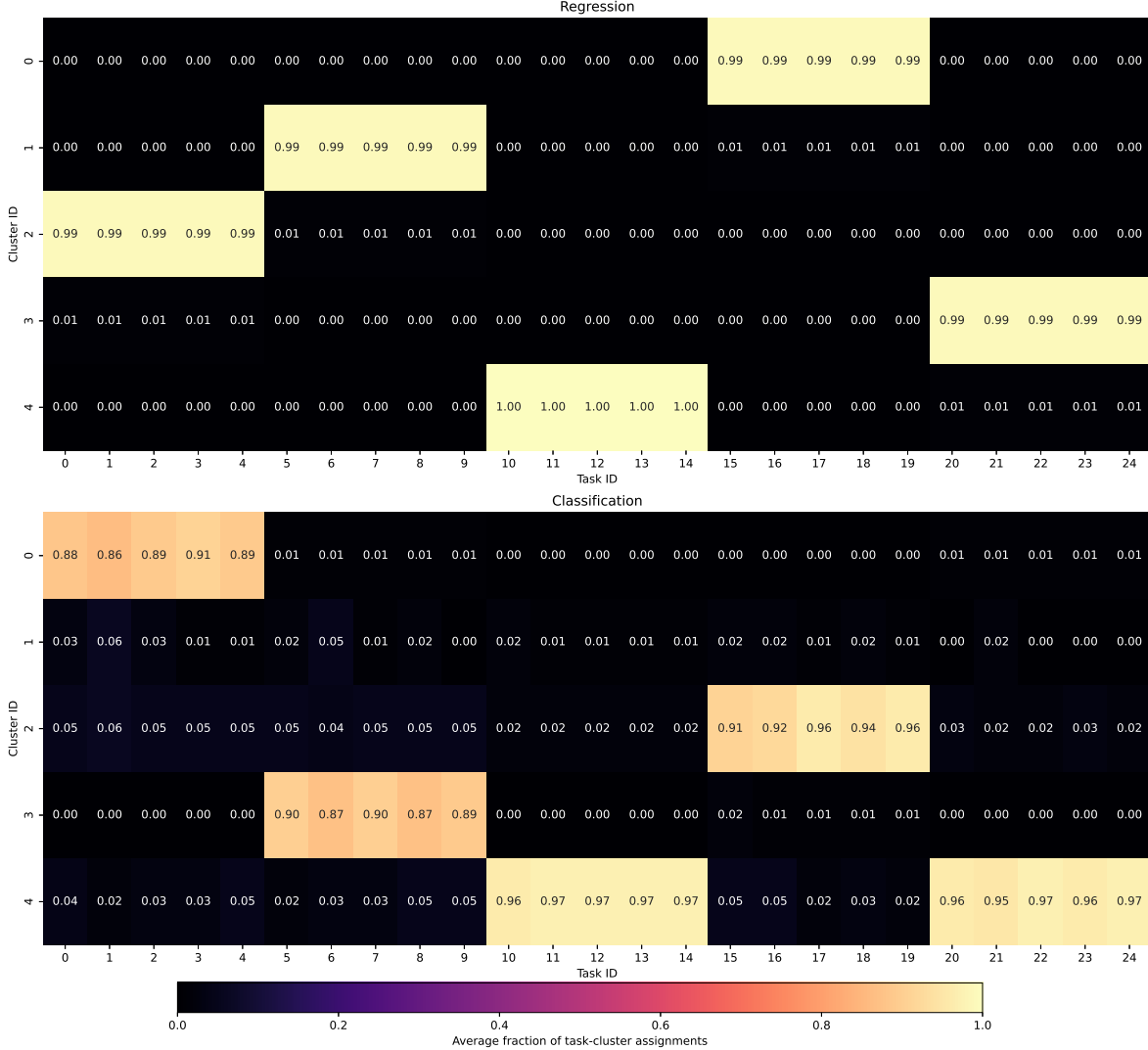


Figure 3: Cluster assignment stability over 100 runs. Each panel shows the fraction of times a task is assigned to each inferred cluster. Columns denote tasks and rows denote clusters; brighter colors indicate more stable assignments. Ground-truth clusters are reported in Table 8.

runs and rows to tasks, with color intensity representing the magnitude of  $\sigma(\theta_i)$  for each task. Rather than revealing a consistent pattern that reflects the underlying multi-cluster structure of the synthetic data, Figure 4 shows highly heterogeneous and unstable weight assignments in the heatmaps. Tasks that belong to the same ground-truth cluster often receive different weights across runs, while tasks from distinct clusters frequently overlap in their  $\sigma(\theta)$  values. This lack of coherence indicates that the sigmoid gating mechanism does not converge to a meaningful partition when more than two task groups are present. Instead, the optimization oscillates between competing binary explanations of the task landscape, leading to run-dependent and task-agnostic weight configurations.

#### 4.4 Real-world results

Regarding the real-world datasets, Tables 9 and 10 report classification performance in terms of accuracy and macro-averaged recall, respectively, while Tables 11 and 12 summarize regression results using **RMSE** and **MAE**. All results are reported as the mean and **Std Dev**, where performance is first averaged across all tasks for each dataset and then averaged over 100 independent runs. The best-performing method for each dataset is highlighted in **bold**.

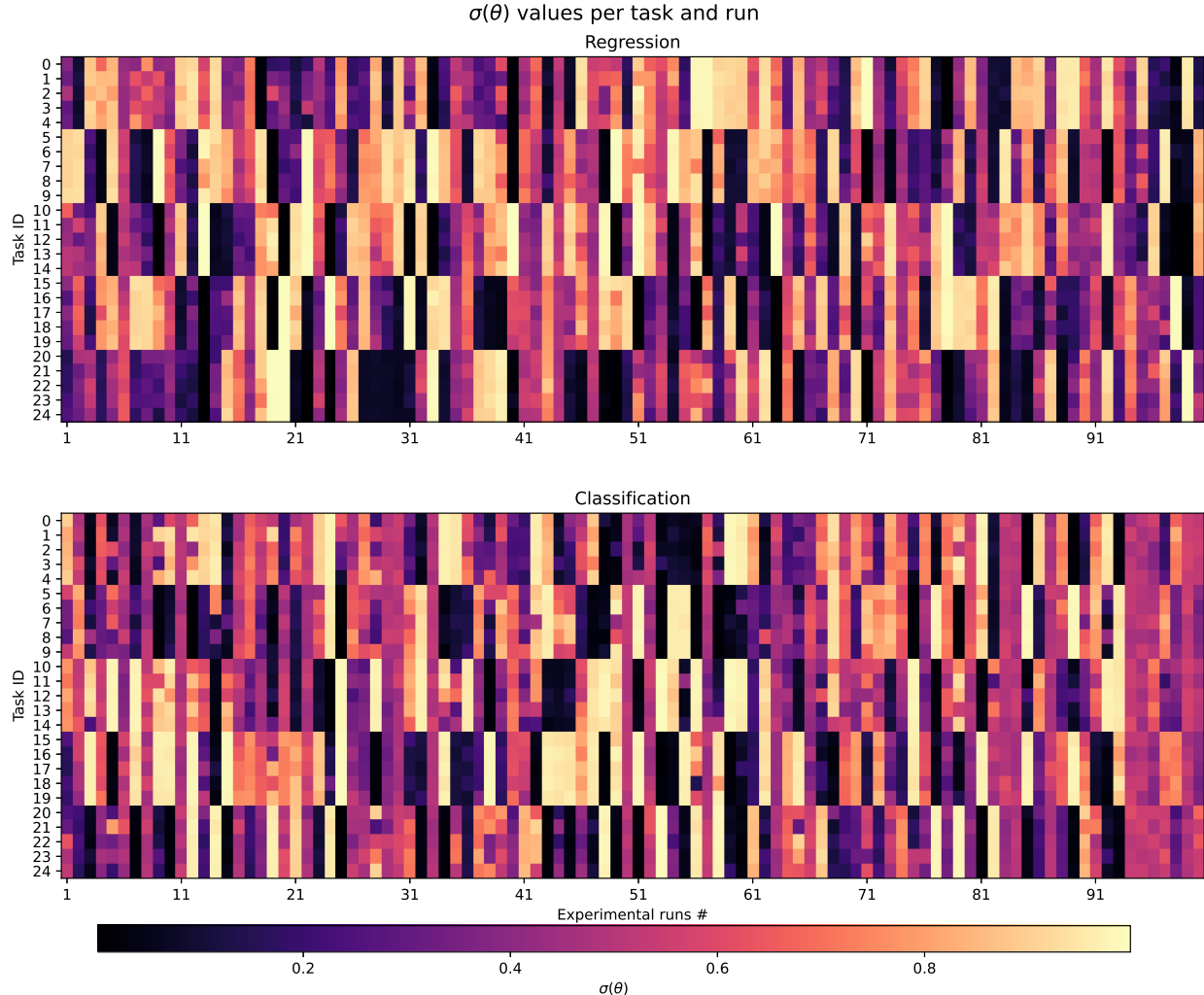


Figure 4: Stability of sigmoid-based task weighting in R-MTGB over 100 runs. Each panel shows the learned task ( $i$ ) weights  $\sigma(\theta_i)$  across runs. Columns denote runs and rows denote tasks; color intensity reflects the magnitude of  $\sigma(\theta_i)$ , indicating how strongly tasks are weighted.

Consistent with the synthetic experiments, the proposed framework utilizing LGBM achieves superior results across all classification datasets (Tables 9 and 10). The low **Std Dev** values indicate that this improvement is not at the expense of stability. In addition, we computed the F1-score (reported in B.3) to assess model performance under class imbalance, and the results show that the proposed framework consistently achieves superior precision-recall balance compared to the studied baselines.

For regression datasets, Tables 11 and 12 show that **MT** approaches, particularly RMB-CLE-via-LGBM, generally achieve the lowest **RMSE**, confirming the advantage of task clustering. An exception is the *Parkinson* dataset, where **ST-GB** attains the best result, with a marginal. Notably, **DP** approaches perform poorly in datasets with many tasks (e.g., *SARCOS* and *Parkinson*).

To further assess performance at the task level on real-world datasets, we follow the same task-wise statistical comparison protocol used in the synthetic experiments (Subsection 4.3) and analyze the relative ranking of methods across tasks. Figure 5 reports the average ranks of task-wise methods computed over individual tasks, where lower ranks indicate better performance. Horizontal bars connect methods whose differences in average rank are not statistically significant at the 5% level, as determined by the **CD**. The results show that, consistent with the synthetic results, the proposed approach achieves the best average rank across both classification (left subplot) and regression tasks (right subplot), and is statistically separated from most

Table 9: Real-world classification accuracy (mean  $\pm$  Std Dev). Best results in bold.

Model	Adult-Gender	Adult-Race	Avila	Bank	Landmine
DP-GB	0.837 $\pm$ 0.005	0.837 $\pm$ 0.005	0.494 $\pm$ 0.010	0.889 $\pm$ 0.003	0.939 $\pm$ 0.003
DP-LGBM	0.854 $\pm$ 0.004	0.854 $\pm$ 0.004	0.536 $\pm$ 0.021	0.898 $\pm$ 0.003	0.939 $\pm$ 0.003
RMB-CLE-via-LGBM	<b>0.872 <math>\pm</math> 0.003</b>	<b>0.873 <math>\pm</math> 0.003</b>	<b>0.875 <math>\pm</math> 0.149</b>	<b>0.906 <math>\pm</math> 0.003</b>	<b>0.946 <math>\pm</math> 0.004</b>
RMB-CLE-via-MTGB	0.848 $\pm$ 0.004	0.837 $\pm$ 0.007	0.604 $\pm$ 0.055	0.894 $\pm$ 0.003	0.943 $\pm$ 0.004
MTGB	0.848 $\pm$ 0.004	0.845 $\pm$ 0.004	0.614 $\pm$ 0.050	0.893 $\pm$ 0.003	0.943 $\pm$ 0.004
R-MTGB	0.849 $\pm$ 0.004	0.849 $\pm$ 0.004	0.619 $\pm$ 0.047	0.895 $\pm$ 0.003	0.943 $\pm$ 0.004
ST-GB	0.841 $\pm$ 0.004	0.838 $\pm$ 0.004	0.610 $\pm$ 0.060	0.892 $\pm$ 0.003	0.942 $\pm$ 0.003
ST-LGBM	0.855 $\pm$ 0.003	0.852 $\pm$ 0.004	0.690 $\pm$ 0.092	0.897 $\pm$ 0.003	0.940 $\pm$ 0.003
TaF-GB	0.837 $\pm$ 0.005	0.837 $\pm$ 0.005	0.497 $\pm$ 0.009	0.889 $\pm$ 0.003	0.939 $\pm$ 0.003
TaF-LGBM	0.854 $\pm$ 0.004	0.854 $\pm$ 0.004	0.552 $\pm$ 0.114	0.898 $\pm$ 0.003	0.939 $\pm$ 0.003

Table 10: Real-world classification recall (mean  $\pm$  Std Dev). Best results in bold.

Model	Adult-Gender	Adult-Race	Avila	Bank	Landmine
DP-GB	0.684 $\pm$ 0.010	0.684 $\pm$ 0.010	0.166 $\pm$ 0.008	0.532 $\pm$ 0.004	0.500 $\pm$ 0.000
DP-LGBM	0.739 $\pm$ 0.005	0.739 $\pm$ 0.005	0.263 $\pm$ 0.025	0.610 $\pm$ 0.006	0.503 $\pm$ 0.003
RMB-CLE-via-LGBM	<b>0.796 <math>\pm</math> 0.005</b>	<b>0.797 <math>\pm</math> 0.005</b>	<b>0.774 <math>\pm</math> 0.182</b>	<b>0.708 <math>\pm</math> 0.010</b>	<b>0.591 <math>\pm</math> 0.014</b>
RMB-CLE-via-MTGB	0.720 $\pm$ 0.005	0.684 $\pm$ 0.018	0.446 $\pm$ 0.083	0.587 $\pm$ 0.011	0.552 $\pm$ 0.010
MTGB	0.720 $\pm$ 0.005	0.716 $\pm$ 0.008	0.438 $\pm$ 0.085	0.576 $\pm$ 0.010	0.549 $\pm$ 0.010
R-MTGB	0.726 $\pm$ 0.006	0.725 $\pm$ 0.005	0.436 $\pm$ 0.083	0.590 $\pm$ 0.009	0.548 $\pm$ 0.011
ST-GB	0.705 $\pm$ 0.006	0.693 $\pm$ 0.008	0.454 $\pm$ 0.088	0.555 $\pm$ 0.005	0.552 $\pm$ 0.010
ST-LGBM	0.744 $\pm$ 0.005	0.737 $\pm$ 0.005	0.589 $\pm$ 0.122	0.617 $\pm$ 0.007	0.524 $\pm$ 0.007
TaF-GB	0.684 $\pm$ 0.010	0.684 $\pm$ 0.010	0.169 $\pm$ 0.007	0.532 $\pm$ 0.004	0.500 $\pm$ 0.000
TaF-LGBM	0.739 $\pm$ 0.005	0.739 $\pm$ 0.005	0.347 $\pm$ 0.135	0.610 $\pm$ 0.006	0.502 $\pm$ 0.003

competing baselines in regression setting. Among the remaining methods, **ST-LGBM** attains the next best ranking for classification problem, while **ST-GB** performs best among the baselines for regression problem, though both remain inferior to the proposed framework in terms of average rank.

## 5 Conclusions

This work introduced Robust Multi-Task Boosting using Clustering and Local Ensembling (**RMB-CLE**), a robust multi-task boosting framework that reframes task relatedness as a question of cross-task generalization rather than in-domain performance or heuristic similarity. By grounding task similarity in error-driven transfer behavior and combining it with adaptive hierarchical clustering and cluster-wise local ensembling, **RMB-CLE** moves beyond the binary inlier-outlier paradigm and provides a systematic mechanism for discovering multiple task groups under heterogeneity.

From a methodological standpoint, the main contribution of **RMB-CLE** lies in its structural treatment of negative transfer. Rather than addressing multi-task generalization through soft weighting or gradient manipulation within a shared model, the proposed framework separates incompatible tasks while preserving

Table 11: Real-world regression RMSE (mean  $\pm$  Std Dev). Best results in bold.

Model	Abalone	Computer	Parkinson	SARCOS	School
DP-GB	2.397 $\pm$ 0.093	2.466 $\pm$ 0.048	8.859 $\pm$ 0.137	18.397 $\pm$ 0.067	10.423 $\pm$ 0.118
DP-LGBM	2.403 $\pm$ 0.093	2.466 $\pm$ 0.048	8.859 $\pm$ 0.136	18.395 $\pm$ 0.067	10.424 $\pm$ 0.118
RMB-CLE-via-LGBM	<b>2.169<math>\pm</math>0.085</b>	<b>2.420<math>\pm</math>0.087</b>	0.349 $\pm$ 0.035	<b>2.507<math>\pm</math>0.020</b>	<b>10.056<math>\pm</math>0.116</b>
RMB-CLE-via-MTGB	2.465 $\pm$ 0.081	2.754 $\pm$ 0.333	1.277 $\pm$ 0.085	10.776 $\pm$ 0.049	10.509 $\pm$ 0.124
MTGB	2.289 $\pm$ 0.087	2.486 $\pm$ 0.047	0.336 $\pm$ 0.024	4.808 $\pm$ 0.034	10.154 $\pm$ 0.122
R-MTGB	2.266 $\pm$ 0.086	2.463 $\pm$ 0.076	0.289 $\pm$ 0.037	4.698 $\pm$ 0.066	10.133 $\pm$ 0.119
ST-GB	2.346 $\pm$ 0.089	2.760 $\pm$ 0.352	<b>0.268<math>\pm</math>0.027</b>	4.919 $\pm$ 0.034	10.295 $\pm$ 0.137
ST-LGBM	2.345 $\pm$ 0.089	2.948 $\pm$ 0.214	0.557 $\pm$ 0.035	4.926 $\pm$ 0.034	10.669 $\pm$ 0.131
TaF-GB	2.383 $\pm$ 0.093	2.467 $\pm$ 0.067	6.559 $\pm$ 0.087	11.266 $\pm$ 0.060	10.415 $\pm$ 0.117
TaF-LGBM	2.388 $\pm$ 0.093	2.469 $\pm$ 0.048	6.558 $\pm$ 0.087	11.266 $\pm$ 0.060	10.416 $\pm$ 0.118

Table 12: Real-world regression MAE (mean  $\pm$  Std Dev). Best results in bold.

Model	Abalone	Computer	Parkinson	SARCOS	School
DP-GB	$1.732 \pm 0.050$	$2.025 \pm 0.043$	$7.340 \pm 0.118$	$12.650 \pm 0.047$	$8.270 \pm 0.097$
DP-LGBM	$1.737 \pm 0.051$	$2.025 \pm 0.043$	$7.339 \pm 0.117$	$12.648 \pm 0.047$	$8.270 \pm 0.098$
RMB-CLE-via-LGBM	<b><math>1.524 \pm 0.046</math></b>	<b><math>1.972 \pm 0.071</math></b>	$0.203 \pm 0.014$	<b><math>1.473 \pm 0.012</math></b>	<b><math>7.938 \pm 0.093</math></b>
RMB-CLE-via-MTGB	$1.882 \pm 0.070$	$2.200 \pm 0.298$	$0.850 \pm 0.059$	$7.159 \pm 0.028$	$8.351 \pm 0.109$
MTGB	$1.624 \pm 0.047$	$2.054 \pm 0.044$	$0.186 \pm 0.015$	$2.778 \pm 0.016$	$8.031 \pm 0.095$
R-MTGB	$1.607 \pm 0.046$	$2.020 \pm 0.068$	$0.137 \pm 0.029$	$2.734 \pm 0.033$	$8.006 \pm 0.094$
ST-GB	$1.664 \pm 0.048$	$2.197 \pm 0.317$	<b><math>0.110 \pm 0.008</math></b>	$2.778 \pm 0.015$	$8.146 \pm 0.108$
ST-LGBM	$1.664 \pm 0.048$	$2.432 \pm 0.194$	$0.301 \pm 0.015$	$2.780 \pm 0.016$	$8.460 \pm 0.112$
TaF-GB	$1.711 \pm 0.050$	$2.043 \pm 0.056$	$5.713 \pm 0.088$	$7.132 \pm 0.031$	$8.270 \pm 0.098$
TaF-LGBM	$1.715 \pm 0.050$	$2.028 \pm 0.043$	$5.712 \pm 0.088$	$7.130 \pm 0.030$	$8.269 \pm 0.098$

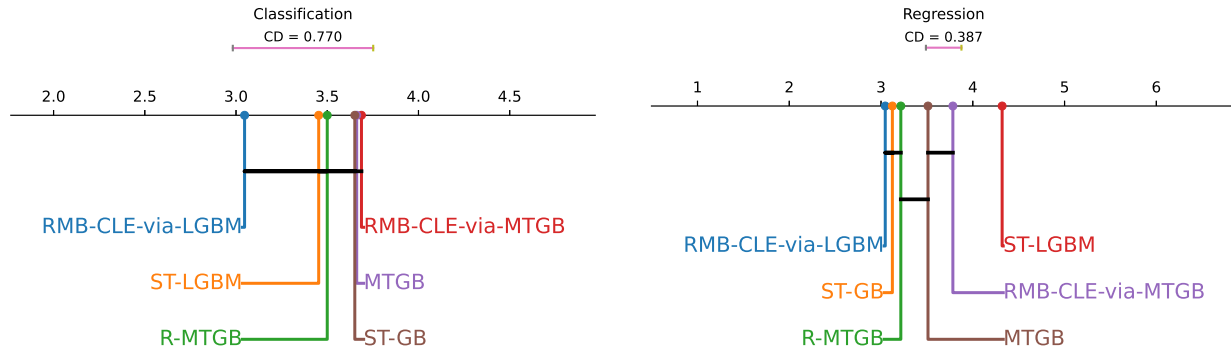


Figure 5: Real-world task-wise Demšar plots ( $p = 0.05$ ) comparing multi-task models; solid lines indicate no significant differences (Nemenyi).

effective knowledge sharing among related ones. This is achieved through three components: (i) cross-task error evaluation as a reference for functional similarity, (ii) unsupervised discovery of latent task clusters without metadata or predefined assumptions, and (iii) cluster-specific ensemble learning that balances robustness and specialization. Moreover, from a theoretical standpoint, **RMB-CLE** is grounded in the fact that cross-task generalization error provides a justified measure of task compatibility. In regression, cross-task risk decomposes into a functional mismatch term and an irreducible noise component, while in classification it upper-bounds the excess risk induced by transferring a model across tasks.

Extensive empirical results on both synthetic and real-world benchmarks demonstrate that **RMB-CLE** consistently improves predictive performance across classification and regression settings. On synthetic data, the framework reliably recovers ground-truth task clusters and achieves performance indistinguishable from oracle cluster-known baselines. On real-world datasets, **RMB-CLE** outperforms single-task learning, naive pooling, and existing multi-task boosting methods, while maintaining stable performance under varying numbers of tasks, class imbalance, and distributional shift. Task-wise statistical tests further confirm that these gains are not driven by a small subset of tasks but reflect systematic improvements.

Ablation studies, reported in the appendices, reinforce the central design choices of the framework. In particular, clustering based on cross-task errors consistently outperforms alternatives based on pseudo-residuals, highlighting the importance of capturing long-run transferability rather than local optimization dynamics. Moreover, the method is robust to the choice of hierarchical linkage criterion, and silhouette-based model selection eliminates the need for manual specification of the number of task clusters.

In summary, **RMB-CLE** establishes a general and scalable principle for robust multi-task learning with ensembles: task structure should be inferred from how models transfer across tasks, rather than from how well they perform in isolation. While the proposed framework is effective for moderate numbers of tasks, its reliance on cross-task evaluation introduces a quadratic dependency on the number of tasks, which motivates the development of more scalable approximations for large-scale settings. In addition, the current formulation assumes a common input dimension across tasks and does not address heterogeneity in task dimensionality, which may arise in applications with partially overlapping or task-specific feature spaces.

Another promising direction is to refine cross-task similarity estimation by accounting for task difficulty, for example by normalizing transfer errors relative to the intrinsic difficulty of the source and target tasks. Addressing these limitations opens several promising directions for future work.

## Declaration of competing interest

The authors report no conflicts of interest or personal relationships that may have influenced the research, experimental work, or the conclusions of this study.

## Acknowledgments

The authors acknowledge financial support from project PID2022-139856NB-I00 (MCIN/AEI/10.13039/501100011033 and FEDER, UE), project IDEA-CM (TEC-2024/COM-89, Comunidad de Madrid), and the ELLIS Unit Madrid, as well as computational resources from the Centro de Computación Científica, Universidad Autónoma de Madrid (CCC-UAM).

## Data and Code availability

The datasets used in this study were obtained from the publicly available sources cited in the references. Both the datasets and the source code developed for the proposed model are publicly accessible at [github.com/GAA-UAM/RMB-CLE](https://github.com/GAA-UAM/RMB-CLE). The generated synthetic datasets are also archived and publicly accessible via Mendeley Data at [data.mendeley.com/datasets/3gms2fv93/](https://data.mendeley.com/datasets/3gms2fv93/).

## References

- [1] Yu Zhang and Qiang Yang. A Survey on Multi-Task Learning. *IEEE Transactions on Knowledge and Data Engineering*, 34(12):5586–5609, 2022.
- [2] Rich Caruana. Multitask Learning. *Machine Learning*, 28(1):41–75, 1997.
- [3] Sara Taylor, Natasha Jaques, Ehimwenma Nosakhare, Akane Sano, and Rosalind Picard. Personalized multitask learning for predicting tomorrow’s mood, stress, and health. *IEEE Transactions on Affective Computing*, 11(2):200–213, 2020.
- [4] Xuejun Liao and Lawrence Carin. Radial Basis Function Network for Multi-task Learning. In *Advances in Neural Information Processing Systems*, volume 18. MIT Press, 2005.
- [5] Daniel L. Silver, Ryan Poirier, and Duane Currie. Inductive transfer with context-sensitive neural networks. *Machine Learning*, 73(3):313–336, 2008.
- [6] Pinghua Gong, Jieping Ye, and Changshui Zhang. Robust multi-task feature learning. In *Proceedings of the 18th ACM SIGKDD international conference on Knowledge discovery and data mining*, pages 895–903, 2012.
- [7] Lei Han, Yu Zhang, Guojie Song, and Kunqing Xie. Encoding Tree Sparsity in Multi-Task Learning: A Probabilistic Framework. In *Proceedings of the AAAI Conference on Artificial Intelligence*, volume 28, 2014.
- [8] Rie Kubota Ando, Tong Zhang, and Peter Bartlett. A framework for learning predictive structures from multiple tasks and unlabeled data. *Journal of machine learning research*, 6(11), 2005.
- [9] Jianhui Chen, Lei Tang, Jun Liu, and Jieping Ye. A convex formulation for learning shared structures from multiple tasks. In *Proceedings of the 26th Annual International Conference on Machine Learning*, pages 137–144. Association for Computing Machinery, 2009.
- [10] Arvind Agarwal, Samuel Gerber, and Hal Daume. Learning Multiple Tasks using Manifold Regularization. In *Advances in Neural Information Processing Systems*, volume 23. Curran Associates, Inc., 2010.
- [11] Sebastian Thrun and Joseph O’Sullivan. Discovering structure in multiple learning tasks: The TC algorithm. In *ICML*, volume 96, pages 489–497. Citeseer, 1996.
- [12] Bart Bakker and Tom Heskes. Task clustering and gating for bayesian multitask learning. *Journal of Machine Learning Research*, 4:83–99, 2003.

- [13] Ya Xue, Xuejun Liao, Lawrence Carin, and Balaji Krishnapuram. Multi-Task Learning for Classification with Dirichlet Process Priors. *Journal of Machine Learning Research*, 8(1), 2007.
- [14] Theodoros Evgeniou and Massimiliano Pontil. Regularized multi-task learning. In *Proceedings of the Tenth ACM SIGKDD International Conference on Knowledge Discovery and Data Mining*, pages 109–117. Association for Computing Machinery, 2004.
- [15] Shabin Parameswaran and Kilian Q Weinberger. Large Margin Multi-Task Metric Learning. In *Advances in Neural Information Processing Systems*, volume 23. Curran Associates, Inc., 2010.
- [16] Nico Goernitz, Christian Widmer, Georg Zeller, Andre Kahles, Gunnar Rätsch, and Sören Sonnenburg. Hierarchical Multitask Structured Output Learning for Large-scale Sequence Segmentation. In *Advances in Neural Information Processing Systems*, volume 24. Curran Associates, Inc., 2011.
- [17] Ali Jalali, Sujay Sanghavi, Chao Ruan, and Pradeep Ravikumar. A Dirty Model for Multi-task Learning. In *Advances in Neural Information Processing Systems*, volume 23. Curran Associates, Inc., 2010.
- [18] Lei Han and Yu Zhang. Learning Tree Structure in Multi-Task Learning. In *Proceedings of the 21th ACM SIGKDD International Conference on Knowledge Discovery and Data Mining*, pages 397–406. Association for Computing Machinery, 2015.
- [19] Qiang Zhou and Qi Zhao. Flexible Clustered Multi-Task Learning by Learning Representative Tasks. *IEEE Transactions on Pattern Analysis and Machine Intelligence*, 38(2):266–278, 2016.
- [20] Eric Backer and Anil K. Jain. A Clustering Performance Measure Based on Fuzzy Set Decomposition. *IEEE Transactions on Pattern Analysis and Machine Intelligence*, PAMI-3(1):66–75, 1981.
- [21] Rui Xu and D. Wunsch. Survey of clustering algorithms. *IEEE Transactions on Neural Networks*, 16(3):645–678, 2005.
- [22] Lior Rokach and Oded Maimon. *Clustering Methods*, pages 321–352. Springer US, 2005.
- [23] An-An Liu, Yu-Ting Su, Wei-Zhi Nie, and Mohan Kankanhalli. Hierarchical Clustering Multi-Task Learning for Joint Human Action Grouping and Recognition. *IEEE Transactions on Pattern Analysis and Machine Intelligence*, 39(1):102–114, 2017.
- [24] Xin Jin and Jiawei Han. *K-Means Clustering*, pages 563–564. Springer US, 2010.
- [25] Jerome H. Friedman. Greedy Function Approximation: A Gradient Boosting Machine. *The Annals of Statistics*, 29(5):1189–1232, 2001.
- [26] Candice Bentéjac, Anna Csörgő, and Gonzalo Martínez-Mu noz. A comparative analysis of gradient boosting algorithms. *Artificial Intelligence Review*, 54(3):1937–1967, 2021.
- [27] Ravid Shwartz-Ziv and Amitai Armon. Tabular data: Deep learning is not all you need. *Information Fusion*, 81:84–90, 2022.
- [28] Tianqi Chen and Carlos Guestrin. XGBoost: A Scalable Tree Boosting System. In *Proceedings of the 22nd ACM SIGKDD International Conference on Knowledge Discovery and Data Mining*, pages 785–794. Association for Computing Machinery, 2016.
- [29] Guolin Ke, Qi Meng, Thomas Finley, Taifeng Wang, Wei Chen, Weidong Ma, Qiwei Ye, and Tie-Yan Liu. LightGBM: A Highly Efficient Gradient Boosting Decision Tree. In *Advances in Neural Information Processing Systems*, volume 30. Curran Associates, Inc., 2017.
- [30] Liudmila Prokhorenkova, Gleb Gusev, Aleksandr Vorobev, Anna Veronika Dorogush, and Andrey Gulin. CatBoost: unbiased boosting with categorical features. In *Advances in Neural Information Processing Systems*, volume 31. Curran Associates, Inc., 2018.
- [31] Olivier Chapelle, Pannagadatta Shivaswamy, Srinivas Vadrevu, Kilian Weinberger, Ya Zhang, and Belle Tseng. Boosted multi-task learning. *Machine Learning*, 85(1-2):149–173, 2011.
- [32] Seyedamani Emami, Carlos Ruiz Pastor, and Gonzalo Martínez-Muñoz. Multi-task gradient boosting. In *Hybrid Artificial Intelligent Systems*, pages 97–107. Springer International Publishing, 2023.
- [33] Seyedamani Emami, Gonzalo Martínez-Mu noz, and Daniel Hernández-Lobato. Robust-multi-task gradient boosting. *Expert Systems with Applications*, 303:130696, 2026. ISSN 0957-4174.
- [34] Shipeng Yu, Volker Tresp, and Kai Yu. Robust multi-task learning with t-processes. In *Proceedings of the 24th International Conference on Machine Learning*, pages 1103–1110. Association for Computing Machinery, 2007.

[35] Laurent Jacob, Jean-philippe Vert, and Francis Bach. Clustered Multi-Task Learning: A Convex Formulation. In *Advances in Neural Information Processing Systems*, volume 21. Curran Associates, Inc., 2008.

[36] Quanquan Gu and Jie Zhou. Learning the Shared Subspace for Multi-task Clustering and Transductive Transfer Classification. In *2009 Ninth IEEE International Conference on Data Mining*, pages 159–168, 2009.

[37] Quanquan Gu, Zhenhui Li, and Jiawei Han. Learning a kernel for multi-task clustering. In *Proceedings of the AAAI Conference on Artificial Intelligence*, volume 25, pages 368–373, 2011.

[38] Jiayu Zhou, Jianhui Chen, and Jieping Ye. Clustered Multi-Task Learning Via Alternating Structure Optimization. In *Advances in Neural Information Processing Systems*, volume 24. Curran Associates, Inc., 2011.

[39] Xiao-Lei Zhang. Convex Discriminative Multitask Clustering. *IEEE Transactions on Pattern Analysis and Machine Intelligence*, 37(1):28–40, 2015.

[40] Yang Yang, Zhigang Ma, Yi Yang, Feiping Nie, and Heng Tao Shen. Multitask Spectral Clustering by Exploring Intertask Correlation. *IEEE Transactions on Cybernetics*, 45(5):1083–1094, 2015.

[41] Xianchao Zhang, Xiaotong Zhang, and Han Liu. Self-Adapted Multi-Task Clustering. In *IJCAI*, pages 2357–2363, 2016.

[42] Xiaotong Zhang, Xianchao Zhang, Han Liu, and Jiebo Luo. Multi-Task Clustering with Model Relation Learning. In *IJCAI*, pages 3132–3140, 2018.

[43] Ozan Sener and Vladlen Koltun. Multi-Task Learning as Multi-Objective Optimization. In *Advances in Neural Information Processing Systems*, volume 31. Curran Associates, Inc., 2018.

[44] Tianhe Yu, Saurabh Kumar, Abhishek Gupta, Sergey Levine, Karol Hausman, and Chelsea Finn. Gradient Surgery for Multi-Task Learning. In *Advances in Neural Information Processing Systems*, volume 33, pages 5824–5836. Curran Associates, Inc., 2020.

[45] Bo Liu, Xingchao Liu, Xiaojie Jin, Peter Stone, and Qiang Liu. Conflict-Averse Gradient Descent for Multi-task learning. In *Advances in Neural Information Processing Systems*, volume 34, pages 18878–18890. Curran Associates, Inc., 2021.

[46] Amir R. Zamir, Alexander Sax, William Shen, Leonidas J. Guibas, Jitendra Malik, and Silvio Savarese. Taskonomy: Disentangling Task Transfer Learning. In *Proceedings of the IEEE Conference on Computer Vision and Pattern Recognition (CVPR)*, 2018.

[47] Trevor Standley, Amir Zamir, Dawn Chen, Leonidas Guibas, Jitendra Malik, and Silvio Savarese. Which Tasks Should Be Learned Together in Multi-task Learning? In *Proceedings of the 37th International Conference on Machine Learning*, volume 119, pages 9120–9132. PMLR, 2020.

[48] Robert R. Sokal and Charles D. Michener. A statistical method for evaluating systematic relationships. *University of Kansas Scientific Bulletin*, 38(2):1409–1438, 1958.

[49] Peter J. Rousseeuw. Silhouettes: A graphical aid to the interpretation and validation of cluster analysis. *Journal of Computational and Applied Mathematics*, 20:53–65, 1987.

[50] Fionn Murtagh and Pedro Contreras. Algorithms for hierarchical clustering: an overview, II. *WIREs Data Mining and Knowledge Discovery*, 7(6):e1219, 2017.

[51] Ali Rahimi and Benjamin Recht. Random Features for Large-Scale Kernel Machines. In *Advances in Neural Information Processing Systems*, volume 20. Curran Associates, Inc., 2007.

[52] Christopher KI Williams and Carl Edward Rasmussen. *Gaussian processes for machine learning*, volume 2. MIT press Cambridge, MA, 2006.

[53] Mengchen Zhao, Bo An, Yaodong Yu, Sulin Liu, and Sinno Pan. Data Poisoning Attacks on Multi-Task Relationship Learning. In *Proceedings of the AAAI Conference on Artificial Intelligence*, volume 32, 2018.

[54] Luca Oneto, Michele Donini, Amon Elders, and Massimiliano Pontil. Taking Advantage of Multitask Learning for Fair Classification. In *Proceedings of the 2019 AAAI/ACM Conference on AI, Ethics, and Society*, pages 227–237. Association for Computing Machinery, 2019.

[55] Yuyan Wang, Xuezhi Wang, Alex Beutel, Flavien Prost, Jilin Chen, and Ed H. Chi. Understanding and Improving Fairness-Accuracy Trade-offs in Multi-Task Learning. In *Proceedings of the 27th ACM SIGKDD Conference on Knowledge Discovery & Data Mining*, pages 1748–1757. Association for Computing Machinery, 2021.

[56] Sinan Wang, Yumeng Li, Hongyan Li, Tanchao Zhu, Zhao Li, and Wenwu Ou. Multi-Task Learning with Calibrated Mixture of Insightful Experts. In *2022 IEEE 38th International Conference on Data Engineering (ICDE)*, pages 3307–3319, 2022.

[57] N.D. Cilia, C. De Stefano, F. Fontanella, C. Marrocco, M. Molinara, and A. Scotto Di Freca. An end-to-end deep learning system for medieval writer identification. *Pattern Recognition Letters*, 129: 137–143, 2020.

[58] S. Moro, R. Laureano, and P. Cortez. Using Data Mining for Bank Direct Marketing: An Application of the CRISP-DM Methodology. In *Proceedings of the European Simulation and Modelling Conference - ESM'2011*, pages 117–121. EUROSIS, 2011.

[59] Hakan Gunduz. Deep Learning-Based Parkinson’s Disease Classification Using Vocal Feature Sets. *IEEE Access*, 7:115540–115551, 2019.

[60] Saravanan Srinivasan, Parthasarathy Ramadass, Sandeep Kumar Mathivanan, Karthikeyan Panneer Selvam, Basu Dev Shivaahare, and Mohd Asif Shah. Detection of Parkinson disease using multiclass machine learning approach. *Scientific Reports*, 14(1):13813, 2024.

[61] Andreas Argyriou, Massimiliano Pontil, Yiming Ying, and Charles Micchelli. A Spectral Regularization Framework for Multi-Task Structure Learning. In *Advances in Neural Information Processing Systems*, volume 20. Curran Associates, Inc., 2007.

[62] C. De Stefano, M. Maniaci, F. Fontanella, and A. Scotto di Freca. Reliable writer identification in medieval manuscripts through page layout features: The “Avila” Bible case. *Engineering Applications of Artificial Intelligence*, 72:99–110, 2018.

[63] Barry Becker and Ronny Kohavi. Adult. <https://archive.ics.uci.edu>, 1996.

[64] Cemal Yilmaz, Hamdi Tolga Kahraman, and Salih Söyler. Passive Mine Detection and Classification Method Based on Hybrid Model. *IEEE Access*, 6:47870–47888, 2018.

[65] Warwick Nash, Tracy Sellers, Simon Talbot, Andrew Cawthorn, and Wes Ford. Abalone. <https://archive.ics.uci.edu>, 1994.

[66] Peter J. Lenk, Wayne S. DeSarbo, Paul E. Green, and Martin R. Young. Hierarchical Bayes Conjoint Analysis: Recovery of Partworth Heterogeneity from Reduced Experimental Designs. *Marketing Science*, 15(2):173–191, 1996.

[67] Athanasios Tsanas and Max Little. Parkinsons Telemonitoring. <https://archive.ics.uci.edu>, 2009.

[68] Pratik Kumar Jawanpuria, Maksim Lapin, Matthias Hein, and Bernt Schiele. Efficient Output Kernel Learning for Multiple Tasks. In *Advances in Neural Information Processing Systems*, volume 28. Curran Associates, Inc., 2015.

[69] Fabian Pedregosa, Gaël Varoquaux, Alexandre Gramfort, Vincent Michel, Bertrand Thirion, Olivier Grisel, Mathieu Blondel, Peter Prettenhofer, Ron Weiss, Vincent Dubourg, et al. Scikit-learn: Machine learning in Python. *the Journal of machine Learning research*, 12:2825–2830, 2011.

[70] Janez Demšar. Statistical comparisons of classifiers over multiple data sets. *The Journal of Machine Learning Research*, 7:1–30, 2006.

## A Ablation study

This ablation study analyzes the main design choices of **RMB-CLE**. First, we examine the impact of the task similarity definition by comparing cross-task error-based similarity with alternative approach (A.1). Second, we study the effect of the clustering strategy, including different linkage criteria in hierarchical clustering (A.2). Third, we investigate the use of pseudo-residual-based similarity matrices as an alternative to cross-task error evaluation (A.3).

### A.1 Alternative out-of-sample approach

An alternative to our cross-task error framework would be to introduce an *out-of-sample* validation procedure within each task. Formally, for every task  $i \in \mathcal{T}$  with dataset  $\mathcal{D}_i = \{(\mathbf{x}_{i,v}, y_{i,v})\}_{v=1}^{n_i}$ , the samples could be partitioned into a training set  $\mathcal{D}_i^{\text{train}}$  and an out-of-sample set  $\mathcal{D}_i^{\text{out}}$ . A task-specific predictor  $F_i$  is then trained on  $\mathcal{D}_i^{\text{train}}$  and evaluated on  $\mathcal{D}_i^{\text{out}}$ , producing residual vectors,

$$\text{error}_i^{\text{out}} = \{y_{i,v} - F_i(\mathbf{x}_{i,v})\}_{v \in \mathcal{D}_i^{\text{out}}}.$$

One could then normalize these residuals and compute a similarity or distance matrix across tasks based on  $\{\text{error}_i^{\text{out}}\}_{i=1}^m$ , which in turn could be used for clustering tasks.

Although such an approach appears natural, we deliberately chose *not* to adopt it for two main reasons:

1. **Data efficiency:** In many tasks, especially those with small sample sizes, splitting into training and out-of-sample subsets reduces the effective sample size used for both model fitting and residual construction. This leads to instability in the estimated residuals  $\text{error}_i^{\text{out}}$ .
2. **Comparability across tasks:** Out-of-sample residuals rely on task-specific holdout splits; so,  $\text{error}_i^{\text{out}}$  and  $\text{error}_j^{\text{out}}$  are defined on different sample supports, with split-specific, task-dependent noise reflected in cross-task distances.

### A.2 Effect of clustering linkage criterion

We repeated all synthetic experiments from Subsection 4.3 using Complete-linkage clustering instead of Average-linkage (UPGMA) to examine whether the choice of linkage criterion affects the formation of task groups. The results remained unchanged. In the regression setting, both linkage methods using **LGBM** produced identical performance, with  $\text{RMSE} = 0.278 \pm 0.017$  and  $\text{MAE} = 0.218 \pm 0.013$ . Likewise, in the classification setting, accuracy and recall were exactly the same under both linkage strategies.

These consistent outcomes indicate that the proposed framework is robust to the choice of hierarchical clustering linkage. This stability arises because the high-level task-group representations do not fluctuate across linkage criteria, and the silhouette-based model selection (Eqs. (10)–(11)) automatically selects the most coherent clustering. Consequently, the method does not rely on manually specifying the number of clusters and remains invariant to linkage variations.

### A.3 Effect of the pseudo-residual

The proposed **RMB-CLE** framework is sensitive to the choice of the input similarity matrix. Rather than computing cross-task errors, one can use pseudo-residuals, which are defined as the *negative gradient* of the loss function ( $\ell$ ) with respect to the model output ( $F_{i,(t-1)}$ ) (See Eq. (4)). Formally, for each training instance of  $v$  of the task  $i$ , the pseudo-residual is given by,

$$\rho_{iv,(t)} = - \frac{\partial \ell(y_{i,v}, F_{i,(t-1)}(\mathbf{x}_{i,v}))}{\partial F_{i,(t-1)}(\mathbf{x}_{i,v})} \bigg|_{F_{i,(t-1)}}. \quad (37)$$

In this subsection we report results obtained when pseudo-residuals are used to build the similarity matrix (Eq. (7)) and we evaluate performance on synthetic (A.3.1) and real-world datasets (A.3.2).

#### A.3.1 Synthetic experiments

Following the setup described in Section 4.1, we generated another 100 repetitions of a synthetic dataset, each containing 25 tasks evenly organized into 5 clusters, constructed using  $\omega = 0.9$ . Each task includes

300 training samples and 1,000 test samples with five input features, evaluated under both classification and regression settings. The studied models were trained and evaluated on these datasets, with **RMB-CLE** constructing the similarity matrix using pseudo-residuals for clustering.

Table 13 presents the performance of the studied models in the synthetic experiment. Comparing these results with Tables 4 and 5, which use cross-task errors for the similarity matrix, we observe that **RMB-CLE** is less effective here than when cross-task errors are used for both classification and regression tasks.

Table 13: Synthetic multi-task results (mean  $\pm$  Std Dev), analogous to Tables 4 and 5, using pseudo-residuals instead of cross-task errors to construct the similarity matrix.

Model	Accuracy	Recall	RMSE	MAE
RMB-CLE-via-LGBM	<b>0.873 <math>\pm</math> 0.019</b>	<b>0.873 <math>\pm</math> 0.019</b>	0.338 $\pm$ 0.020	0.266 $\pm$ 0.015
Cluster-Known-LGBM	<b>0.873 <math>\pm</math> 0.019</b>	<b>0.873 <math>\pm</math> 0.019</b>	0.338 $\pm$ 0.020	0.266 $\pm$ 0.015
Cluster-Known-MTGB	0.818 $\pm$ 0.015	0.818 $\pm$ 0.015	0.336 $\pm$ 0.020	0.264 $\pm$ 0.016
RMB-CLE-via-MTGB	0.818 $\pm$ 0.015	0.818 $\pm$ 0.015	0.336 $\pm$ 0.020	0.264 $\pm$ 0.016
ST-LGBM	0.804 $\pm$ 0.016	0.804 $\pm$ 0.016	<b>0.328 <math>\pm</math> 0.013</b>	<b>0.258 <math>\pm</math> 0.010</b>
ST-GB	0.803 $\pm$ 0.016	0.803 $\pm$ 0.016	0.357 $\pm$ 0.015	0.280 $\pm$ 0.012
R-MTGB	0.733 $\pm$ 0.052	0.733 $\pm$ 0.052	0.540 $\pm$ 0.103	0.431 $\pm$ 0.086
MTGB	0.728 $\pm$ 0.084	0.728 $\pm$ 0.084	0.792 $\pm$ 0.203	0.644 $\pm$ 0.172
DP-GB	0.628 $\pm$ 0.031	0.628 $\pm$ 0.031	0.842 $\pm$ 0.157	0.686 $\pm$ 0.135
TaF-GB	0.628 $\pm$ 0.031	0.628 $\pm$ 0.031	0.547 $\pm$ 0.044	0.435 $\pm$ 0.035
DP-LGBM	0.623 $\pm$ 0.031	0.623 $\pm$ 0.031	0.840 $\pm$ 0.157	0.685 $\pm$ 0.135
TaF-LGBM	0.622 $\pm$ 0.031	0.622 $\pm$ 0.031	0.545 $\pm$ 0.044	0.434 $\pm$ 0.035

The per-task performance of the task-wise models is presented in Figure 6, shown as a Demšar ranking plot with statistical differences measured using the Nemenyi test. The proposed framework, yet clustered using pseudo-residuals consistently achieved the best or second-best rankings in classification problem (left subplot) and the third and fourth positions in regression problem (right subplot). In contrast, conventional boosting-based multi-task models (**R-MTGB** and **MTGB**) obtained the lowest rankings across all problems (subplots).

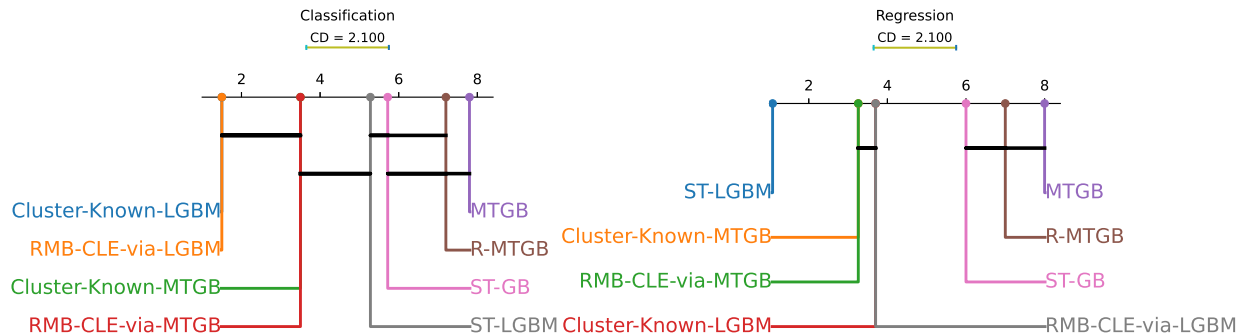


Figure 6: Synthetic task-wise Demšar plots ( $p = 0.05$ ), analogous to Figure 2, where task clustering is performed using pseudo-residuals instead of cross-task errors. Rankings are computed across classification and regression tasks.

### A.3.2 Real-world experiments

Tables 14 and 15 report real-world results for the proposed **RMB-CLE** framework when task clustering is performed using pseudo-residuals (Eq. 37) rather than cross-task errors (Eq. 5). Following the same evaluation protocol as in the real-world experiments (Subsection 4.4), each experiment is repeated 100 times; in each run, performance is first averaged across tasks, and the final results are reported as the mean and **Std Dev** over the 100 runs

Compared to clustering based on cross-task errors, the pseudo-residual variant achieves less stable improvements. While **RMB-CLE** with pseudo-residual clustering can still match or occasionally outperform certain baselines (e.g., on *Adult* and *SARCOS*), its gains are less consistent and, in several cases, inferior to those obtained with the cross-task error-based similarity.

Table 14: Real-world multi-task classification accuracy (mean  $\pm$  Std Dev), analogous to Table 9, using pseudo-residual-based clustering.

Model	Adult-Gender	Adult-Race	Avila	Bank	Landmine
DP-GB	$0.837 \pm 0.005$	$0.837 \pm 0.005$	$0.494 \pm 0.010$	$0.889 \pm 0.003$	$0.939 \pm 0.003$
DP-LGBM	$0.854 \pm 0.004$	$0.854 \pm 0.004$	$0.536 \pm 0.021$	$0.898 \pm 0.003$	$0.939 \pm 0.003$
RMB-CLE-via-LGBM	<b><math>0.872 \pm 0.003</math></b>	<b><math>0.873 \pm 0.003</math></b>	<b><math>0.872 \pm 0.150</math></b>	<b><math>0.902 \pm 0.003</math></b>	$0.941 \pm 0.004$
RMB-CLE-via-MTGB	$0.848 \pm 0.004$	$0.838 \pm 0.005$	$0.604 \pm 0.055$	$0.894 \pm 0.003$	$0.943 \pm 0.004$
MTGB	$0.848 \pm 0.004$	$0.845 \pm 0.004$	$0.614 \pm 0.050$	$0.893 \pm 0.003$	$0.943 \pm 0.004$
R-MTGB	$0.849 \pm 0.004$	$0.849 \pm 0.004$	$0.619 \pm 0.047$	$0.895 \pm 0.003$	<b><math>0.943 \pm 0.004</math></b>
ST-GB	$0.841 \pm 0.004$	$0.838 \pm 0.004$	$0.610 \pm 0.060$	$0.892 \pm 0.003$	$0.942 \pm 0.003$
ST-LGBM	$0.855 \pm 0.003$	$0.852 \pm 0.004$	$0.690 \pm 0.092$	$0.897 \pm 0.003$	$0.940 \pm 0.003$
TaF-GB	$0.837 \pm 0.005$	$0.837 \pm 0.005$	$0.497 \pm 0.009$	$0.889 \pm 0.003$	$0.939 \pm 0.003$
TaF-LGBM	$0.854 \pm 0.004$	$0.854 \pm 0.004$	$0.552 \pm 0.114$	$0.898 \pm 0.003$	$0.939 \pm 0.003$

Table 15: Real-world multi-task regression RMSE (mean  $\pm$  Std Dev), analogous to Table 11, using pseudo-residual-based clustering.

Model	Abalone	Computer	Parkinson	SARCOS	School
DP-GB	$2.397 \pm 0.093$	$2.466 \pm 0.048$	$8.859 \pm 0.137$	$18.397 \pm 0.067$	$10.423 \pm 0.118$
DP-LGBM	$2.403 \pm 0.093$	$2.466 \pm 0.048$	$8.859 \pm 0.136$	$18.395 \pm 0.067$	$10.424 \pm 0.118$
RMB-CLE-via-LGBM	<b><math>2.169 \pm 0.085</math></b>	$2.933 \pm 0.221$	$0.495 \pm 0.039$	<b><math>2.203 \pm 0.016</math></b>	$10.725 \pm 0.128$
RMB-CLE-via-MTGB	$2.465 \pm 0.081$	$2.754 \pm 0.333$	<b><math>0.209 \pm 0.029</math></b>	$7.561 \pm 0.051$	$10.292 \pm 0.139$
MTGB	$2.289 \pm 0.087$	$2.486 \pm 0.047$	$0.336 \pm 0.024$	$4.808 \pm 0.034$	$10.154 \pm 0.122$
R-MTGB	$2.266 \pm 0.086$	<b><math>2.463 \pm 0.076</math></b>	$0.289 \pm 0.037$	$4.698 \pm 0.066$	<b><math>10.133 \pm 0.119</math></b>
ST-GB	$2.346 \pm 0.089$	$2.760 \pm 0.352$	$0.268 \pm 0.027$	$4.919 \pm 0.034$	$10.295 \pm 0.137$
ST-LGBM	$2.345 \pm 0.089$	$2.948 \pm 0.214$	$0.557 \pm 0.035$	$4.926 \pm 0.034$	$10.669 \pm 0.131$
TaF-GB	$2.383 \pm 0.093$	$2.467 \pm 0.067$	$6.559 \pm 0.087$	$11.266 \pm 0.060$	$10.415 \pm 0.117$
TaF-LGBM	$2.388 \pm 0.093$	$2.469 \pm 0.048$	$6.558 \pm 0.087$	$11.266 \pm 0.060$	$10.416 \pm 0.118$

The related task-wise rankings (Figure 7) confirm the results reported in Tables 14 and 15 showing that using pseudo-residuals instead of cross-task errors to construct the similarity matrix does not guarantee that the model will be optimal or achieve better performance.

These observations confirm that the quality of the clustering signal is critical: cross-task errors generally provide a more reliable basis for task grouping than pseudo-residuals. Although the pseudo-residual variant of **RMB-CLE** remains competitive in some settings, it cannot be considered the best-performing approach overall, and its usefulness should be carefully weighed against the residual-based alternative.

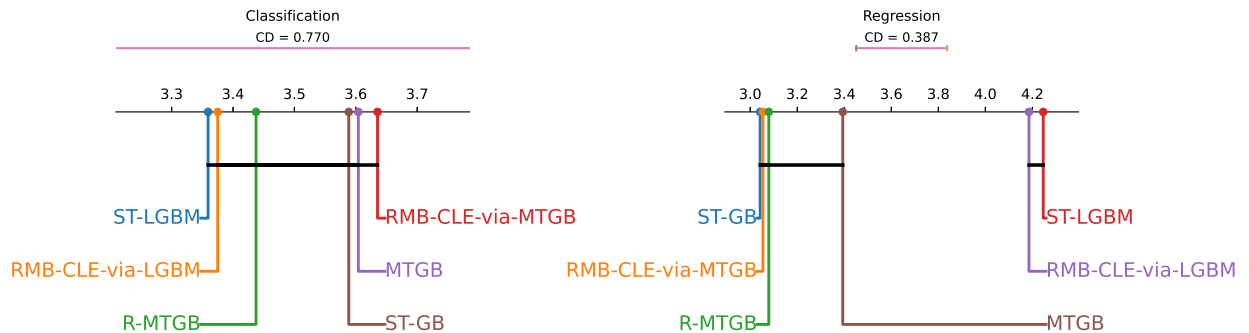


Figure 7: Real-world task-wise Demšar plots ( $p = 0.05$ ), analogous to Figure 5, with task clustering based on pseudo-residuals rather than cross-task errors.

### A.3.3 Discussion and limitations

While clustering based on pseudo-residuals could returns partitions that appear similar to those obtained from cross-task errors, the resulting performance is generally inferior. The reason is that pseudo-residuals capture only local optimization dynamics (gradients of the loss at a given training iteration) rather than long-run transferability between tasks. Consequently, the similarity profiles they generate are less stable, more sensitive to training noise, and do not consistently reflect functional relatedness. Even if the final task assignments were to coincide with those from cross-task errors, the underlying similarity geometry could still differ. For illustration, pseudo-residual similarities might flatten the relative closeness of tasks (e.g., treating  $m_1 \approx m_2 \approx m_3$  instead of the true  $m_1 \approx m_2 < m_3$ ), so that clusters appear correct at the partition level but do not reflect genuine functional relationships. Cross-task errors, by contrast, directly evaluate out-of-domain generalization by testing models trained on one task against another.

One might also consider computing pseudo-residuals in a cross-task fashion (i.e., evaluating residuals from task  $j$  on task  $i$ ). However, this would largely duplicate the information already contained in cross-task errors, while adding instability due to the iteration-dependent nature of residuals and the arbitrary need to select training iterations. Moreover, the clustering signal obtained in this way would still be less reliable, as pseudo-residuals emphasize gradient noise rather than functional similarity. For these reasons, and given the consistent empirical advantage of error-based similarities across our ablations, we restrict the main **RMB-CLE** framework to clustering with cross-task errors.

## B Additional experiments and results

This appendix presents additional experimental analyses that extend the results discussed in Section 4. First, in B.1, we examine the computational costs of the models and approaches under study. Next, we complement this analysis with empirical measurements of elapsed runtime across different scenarios (B.2). Finally, in B.3, we report an additional accuracy metric, the F1-score, to provide insight into the experimental results under class imbalance.

### B.1 Computational Cost

This section analyzes the computational cost of the proposed **RMB-CLE** framework and compares its asymptotic complexity with **GB**, **MTGB**, and **R-MTGB**. We express computational cost in terms of boosting blocks ( $\mathcal{S}_{(.)}$ ), the number of tasks ( $m$ ), and the average number of training instances per task ( $\bar{n}$ ). For each methodology/approach, we report both training and latency complexities using Big- $\mathcal{O}$  notation.

Different boosting blocks  $\mathcal{S}_{(.)}$  are distinguished by their functional role within the learning architecture rather than by their internal optimization mechanism. While all blocks consist of sequential boosting iterations trained in the same manner, their indices indicate the type of information they model and the scope over which they operate. For instance, blocks may correspond to shared learning across tasks ( $\mathcal{S}_{(1)}$ ), task-specific refinement ( $\mathcal{S}_{(2)}$ ), outlier-aware weighting ( $\mathcal{S}_{(3)}$ ), or cluster-level ensembling ( $\mathcal{S}_{(4)}$ ).

#### Training complexity

**Single-Task approaches** Standard **ST** approach consists of a single boosting block of  $\mathcal{K}_{\mathcal{S}_{(2)}}$  base learners. Its training complexity is

$$\mathcal{O}(\mathcal{K}_{\mathcal{S}_{(2)}} \bar{n}).$$

**MTGB** **MTGB** is composed of two sequential boosting blocks: a shared block of  $\mathcal{K}_{\mathcal{S}_{(1)}}$  base learners and a task-specific block of  $\mathcal{K}_{\mathcal{S}_{(2)}}$  base learners. Hence, the training complexity scales as

$$\mathcal{O}((\mathcal{K}_{\mathcal{S}_{(1)}} + \mathcal{K}_{\mathcal{S}_{(2)}}) m \bar{n}).$$

**R-MTGB** This model extends **MTGB** by introducing an additional outlier-aware block  $\mathcal{S}_{(3)}$  between the shared and task-specific blocks, resulting in three sequential blocks of  $\mathcal{K}_{\mathcal{S}_{(1)}}$ ,  $\mathcal{K}_{\mathcal{S}_{(2)}}$ , and  $\mathcal{K}_{\mathcal{S}_{(3)}}$  base learners, with two branches in the third block. Therefore, its training complexity is

$$\mathcal{O}((\mathcal{K}_{\mathcal{S}_{(1)}} + \mathcal{K}_{\mathcal{S}_{(2)}} + 2\mathcal{K}_{\mathcal{S}_{(3)}}) m \bar{n}),$$

which has the same asymptotic order as **MTGB** but with a larger constant factor [33].

**RMB-CLE** The proposed framework follows a different strategy by evaluating task similarity and forming task clusters prior to cluster-wise ensemble training.

- **Initial task-wise boosting:** each task is first modeled independently using task-specific boosting block of  $\mathcal{K}_{\mathcal{S}_{(2)}}$  predictors resulting in

$$\mathcal{O}(\mathcal{K}_{\mathcal{S}_{(2)}} m \bar{n}).$$

- **Cross-task evaluation:** each task model is evaluated on all other tasks to construct the cross-task error matrix, incurring

$$\mathcal{O}(m^2 \bar{n}).$$

- **Similarity computation and clustering:** building the similarity matrix and performing hierarchical clustering costs

$$\mathcal{O}(m^2 \log m).$$

- **Cluster-wise ensemble training:** For each identified cluster, a local boosting ensemble of  $\mathcal{K}_{\mathcal{S}_{(4)}}$  base learners is trained using the pooled data within that cluster. Aggregating over all clusters, the computational complexity of this step is

$$\mathcal{O}(\mathcal{K}_{\mathcal{S}_{(4)}} m \bar{n}).$$

The total training complexity of RMB-CLE is

$$\mathcal{O}((\mathcal{K}_{\mathcal{S}_{(2)}} + \mathcal{K}_{\mathcal{S}_{(4)}}) m \bar{n}) + \mathcal{O}(m^2 \bar{n}) + \mathcal{O}(m^2 \log m).$$

### Latency complexity

At prediction time, prediction for a single test instance requires evaluating the sequence of boosting blocks associated with the corresponding task. Since the number of boosting iterations within each block is fixed after training, latency cost is independent of the number of tasks  $m$  and the average number of training samples  $\bar{n}$ . However, different methods have different constant-time costs depending on the number of boosting blocks and base learners that must be evaluated.

**Single-task approaches** Prediction requires evaluating a single boosting block consisting of  $\mathcal{K}_{\mathcal{S}_{(2)}}$  base learners, resulting in a per-instance latency of

$$\mathcal{O}(\mathcal{K}_{\mathcal{S}_{(2)}}).$$

**MTGB** Prediction involves evaluating both the shared and task-specific boosting blocks, with  $\mathcal{K}_{\mathcal{S}_{(1)}}$  and  $\mathcal{K}_{\mathcal{S}_{(2)}}$  base learners, respectively. The resulting per-instance latency is

$$\mathcal{O}(\mathcal{K}_{\mathcal{S}_{(1)}} + \mathcal{K}_{\mathcal{S}_{(2)}}).$$

**R-MTGB** This model evaluates a shared block, an outlier-aware block with two branches, and a task-specific block. Consequently, prediction requires

$$\mathcal{O}(\mathcal{K}_{\mathcal{S}_{(1)}} + \mathcal{K}_{\mathcal{S}_{(2)}} + 2\mathcal{K}_{\mathcal{S}_{(3)}}),$$

operations per test instance, showing a larger constant factor than **MTGB**.

**RMB-CLE** Given a task identifier, prediction consists of a constant-time cluster lookup followed by evaluation of the corresponding cluster-level ensemble with  $\mathcal{K}_{\mathcal{S}_{(4)}}$  base learners. Therefore, the per-instance latency of is

$$\mathcal{O}(\mathcal{K}_{\mathcal{S}_{(4)}}).$$

A summary of the training and latency complexities of the studied methods and approaches is reported in Table 16.

Table 16: Summary of training and latency complexity for the studied methods.

Method/Approach	Training Complexity	Inference Complexity
Single-Task	$\mathcal{O}(\mathcal{K}_{\mathcal{S}_{(2)}} \bar{n})$	$\mathcal{O}(\mathcal{K}_{\mathcal{S}_{(2)}})$
MTGB	$\mathcal{O}((\mathcal{K}_{\mathcal{S}_{(1)}} + \mathcal{K}_{\mathcal{S}_{(2)}}) m \bar{n})$	$\mathcal{O}(\mathcal{K}_{\mathcal{S}_{(1)}} + \mathcal{K}_{\mathcal{S}_{(2)}})$
R-MTGB	$\mathcal{O}((\mathcal{K}_{\mathcal{S}_{(1)}} + \mathcal{K}_{\mathcal{S}_{(2)}} + 2\mathcal{K}_{\mathcal{S}_{(3)}}) m \bar{n})$	$\mathcal{O}(\mathcal{K}_{\mathcal{S}_{(1)}} + \mathcal{K}_{\mathcal{S}_{(2)}} + 2\mathcal{K}_{\mathcal{S}_{(3)}})$
RMB-CLE	$\mathcal{O}((\mathcal{K}_{\mathcal{S}_{(2)}} + \mathcal{K}_{\mathcal{S}_{(4)}}) m \bar{n}) + \mathcal{O}(m^2 \bar{n}) + \mathcal{O}(m^2 \log m)$	$\mathcal{O}(\mathcal{K}_{\mathcal{S}_{(4)}})$

## B.2 Time evaluation

For each batch of synthetic experiments, we measured elapsed *wall-clock* time (in seconds) using `time.perf_counter` of Python, a high-resolution timer designed for precise performance measurements. For each model configuration, we decomposed the runtime into four components: (i) *grid-search time*, defined as the time required to run the `GridSearch` procedure with cross-validation; (ii) *best-fit time*, corresponding to the time needed to train a single model on the full training set using the hyperparameter configuration selected by the grid search; (iii) *total training time*, computed as the sum of the *grid-search time* and the *best-fit time*; and (iv) *prediction time*, measured as the time required to generate predictions on the test split using the fitted best model. We repeated this procedure over 100 experimental runs (corresponding to 100 independently generated synthetic datasets) and report the mean and `Std Dev` of the per-batch times in Tables 17 and 18 for the classification and regression synthetic datasets, respectively. The best (fastest) result in each column is highlighted in **bold**.

Across both settings, the relative ordering of methods is highly consistent, showing that computational behavior is primarily driven by model architecture rather than problem type. Pooling and single-task baselines, particularly **DP-LGBM**, achieves the lowest runtimes across all components, as they train a single global model (**DP**) or independent task-wise models (**ST**) without multi-stage or cluster-specific structures. **TaF** models experience slightly higher costs due to the augmented input space but remain computationally efficient since they still rely on a single shared ensemble.

In contrast, **MT** boosting methods such as **MTGB** and **R-MTGB** exhibit higher grid-search and training times, reflecting their sequential multi-block architectures. The **MTGB** trains separate shared and task-specific boosting stages, while **R-MTGB** further introduces an outlier-aware block, increasing both the number of boosting stages and the dimensionality of the hyperparameter search. Cluster-based approaches, including the oracle Cluster-Known baselines and the proposed **RMB-CLE** variants, show nearly identical timing profiles when instantiated with the same local ensemble ( $f \in \mathcal{F}$  in Eq. (13)). This is because, once clusters are fixed, both methods reduce to training cluster-specific ensembles on pooled data, and the clustering step itself introduces negligible overhead. Across all methods, configurations based on **LGBM** consistently achieve lower training times due to the histogram-based feature binning and shallow tree construction in **LGBM**, which reduce split-search complexity, memory access costs, and per-iteration computation compared to standard **GB** implementations. Furthermore, **RMB-CLE** avoids the sequential per-task boosting structure of **MTGB** and **R-MTGB** (when **LGBM** is used as the local ensemble), resulting in lower training times while maintaining comparable prediction latency, which remains low due to constant-time cluster lookup followed by a single ensemble evaluation.

While Tables 17 and 18 provide numerical summaries, the substantial differences in magnitude between grid-search, training, and prediction times make it difficult to assess their relative contributions at a glance. To address this, we separate these components into dedicated panels in Figure 8, which presents log-scale visualizations of the mean runtime for regression (top) and classification (bottom). Figure 8 shows that grid-search and best-fit training dominate the total runtime across all methods, with particularly high costs for **R-MTGB**. This behavior reflects its sequential block structure and enlarged hyperparameter space. In contrast, **DP**, **ST**, and **TaF** baselines have lower mean elapsed time due to their simpler training procedures. Prediction time is reported separately, as it is consistently one to two orders of magnitude smaller than training-related costs across all models and is largely insensitive to the underlying architecture. The qualitative runtime patterns are nearly identical for classification and regression.

Table 17: Classification wall-clock time in seconds (mean  $\pm$  Std Dev). Best results in bold.

Model	Grid search time	Best fit time	Total training time	Prediction time
Cluster-Known-LGBM	$7.028 \pm 0.595$	$3.374 \pm 0.373$	$10.402 \pm 0.702$	$0.193 \pm 0.021$
Cluster-Known-MTGB	$21.607 \pm 1.720$	$4.927 \pm 0.668$	$26.534 \pm 1.845$	$0.458 \pm 0.095$
DP-GB	$1.522 \pm 0.140$	$0.757 \pm 0.101$	$2.279 \pm 0.173$	$0.160 \pm 0.022$
DP-LGBM	<b><math>0.139 \pm 0.015</math></b>	<b><math>0.045 \pm 0.009</math></b>	<b><math>0.184 \pm 0.018</math></b>	<b><math>0.057 \pm 0.012</math></b>
RMB-CLE-via-LGBM	$7.013 \pm 0.597$	$3.374 \pm 0.366$	$10.387 \pm 0.700$	$0.193 \pm 0.021$
RMB-CLE-via-MTGB	$21.679 \pm 1.815$	$4.924 \pm 0.671$	$26.603 \pm 1.935$	$0.458 \pm 0.096$
MTGB	$8.589 \pm 0.649$	$2.591 \pm 0.255$	$11.180 \pm 0.698$	$0.862 \pm 0.050$
R-MTGB	$32.456 \pm 2.194$	$3.542 \pm 0.390$	$35.998 \pm 2.229$	$0.892 \pm 0.052$
ST-GB	$4.047 \pm 0.366$	$1.434 \pm 0.194$	$5.481 \pm 0.414$	$0.200 \pm 0.018$
ST-LGBM	$1.737 \pm 0.088$	$0.504 \pm 0.050$	$2.241 \pm 0.101$	$0.070 \pm 0.006$
TaF-GB	$1.824 \pm 0.186$	$0.850 \pm 0.134$	$2.674 \pm 0.229$	$0.195 \pm 0.043$
TaF-LGBM	$0.361 \pm 0.031$	$0.103 \pm 0.023$	$0.463 \pm 0.039$	$0.074 \pm 0.026$

Table 18: Regression wall-clock time in seconds (mean  $\pm$  Std Dev). Best results in bold.

Model	Grid search time	Best fit time	Total training time	Prediction time
Cluster-Known-LGBM	$5.056 \pm 0.342$	$2.424 \pm 0.164$	$7.480 \pm 0.379$	$0.210 \pm 0.010$
Cluster-Known-MTGB	$14.735 \pm 0.996$	$3.484 \pm 0.235$	$18.219 \pm 1.023$	$0.397 \pm 0.035$
DP-GB	$1.197 \pm 0.083$	$0.598 \pm 0.038$	$1.795 \pm 0.091$	$0.086 \pm 0.005$
DP-LGBM	<b><math>0.119 \pm 0.013</math></b>	<b><math>0.038 \pm 0.002</math></b>	<b><math>0.157 \pm 0.013</math></b>	<b><math>0.062 \pm 0.002</math></b>
RMB-CLE-via-LGBM	$5.068 \pm 0.338$	$2.427 \pm 0.159$	$7.495 \pm 0.374$	$0.210 \pm 0.010$
RMB-CLE-via-MTGB	$14.697 \pm 1.006$	$3.484 \pm 0.245$	$18.181 \pm 1.035$	$0.396 \pm 0.035$
MTGB	$6.691 \pm 0.424$	$2.065 \pm 0.131$	$8.756 \pm 0.444$	$0.609 \pm 0.033$
R-MTGB	$24.144 \pm 1.637$	$2.754 \pm 0.201$	$26.899 \pm 1.649$	$0.635 \pm 0.035$
ST-GB	$3.382 \pm 0.167$	$1.267 \pm 0.063$	$4.649 \pm 0.178$	$0.217 \pm 0.013$
ST-LGBM	$1.725 \pm 0.094$	$0.558 \pm 0.038$	$2.282 \pm 0.102$	$0.081 \pm 0.004$
TaF-GB	$1.490 \pm 0.118$	$0.694 \pm 0.062$	$2.184 \pm 0.133$	$0.118 \pm 0.024$
TaF-LGBM	$0.336 \pm 0.017$	$0.098 \pm 0.005$	$0.434 \pm 0.018$	$0.086 \pm 0.032$

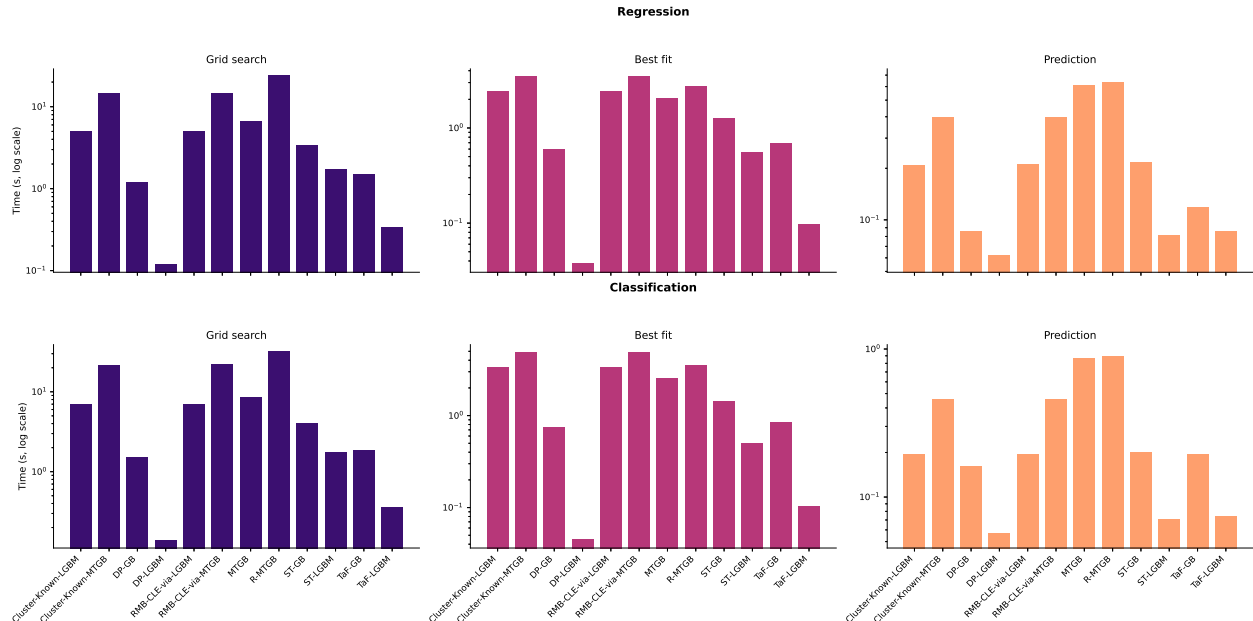


Figure 8: Runtime decomposition (log scale) for regression (top) and classification (bottom), showing mean grid-search, best-fit training, and prediction times over 100 runs for each model.

### B.3 F1-score

In addition to accuracy and recall reported in the experiments described in Subsection 4.4, we also report the F1-score computed using the macro averaging scheme. This provides a balanced evaluation of classification performance under class imbalance and complements the results presented in Tables 9 and 10.

Table 19 reports the mean and [Std Dev](#) of the test F1-score over 100 runs for all real-world multi-task classification datasets. Results are first averaged across tasks and then across repetitions, and the best-performing method for each dataset is highlighted in **bold**. Consistent with the accuracy and recall results presented in Tables 9 and 10, RMB-CLE-via-LGBM achieves the highest F1-score across all datasets, indicating that its performance gains are not driven by a single metric but reflect a robust improvement in the precision-recall balance. In contrast, pooling-based and heuristic [MT](#) baselines exhibit substantially lower F1-scores, particularly on highly imbalanced datasets such as *Avila* and *Landmine*.

Table 19: Real-world classification F1-score (mean  $\pm$  Std Dev). Best results in bold.

Model	Adult-Gender	Adult-Race	Avila	Bank	Landmine
DP-GB	$0.717 \pm 0.011$	$0.717 \pm 0.011$	$0.144 \pm 0.006$	$0.532 \pm 0.007$	$0.484 \pm 0.001$
DP-LGBM	$0.769 \pm 0.005$	$0.769 \pm 0.005$	$0.270 \pm 0.028$	$0.646 \pm 0.008$	$0.490 \pm 0.007$
RMB-CLE-via-LGBM	<b><math>0.814 \pm 0.004</math></b>	<b><math>0.815 \pm 0.004</math></b>	<b><math>0.772 \pm 0.173</math></b>	<b><math>0.738 \pm 0.009</math></b>	<b><math>0.635 \pm 0.019</math></b>
RMB-CLE-via-MTGB	$0.752 \pm 0.006$	$0.717 \pm 0.021$	$0.458 \pm 0.105$	$0.616 \pm 0.015$	$0.577 \pm 0.017$
MTGB	$0.753 \pm 0.005$	$0.748 \pm 0.007$	$0.461 \pm 0.101$	$0.602 \pm 0.014$	$0.573 \pm 0.017$
R-MTGB	$0.758 \pm 0.006$	$0.757 \pm 0.005$	$0.459 \pm 0.097$	$0.620 \pm 0.013$	$0.571 \pm 0.017$
ST-GB	$0.737 \pm 0.006$	$0.726 \pm 0.008$	$0.464 \pm 0.108$	$0.571 \pm 0.008$	$0.577 \pm 0.016$
ST-LGBM	$0.773 \pm 0.005$	$0.767 \pm 0.005$	$0.603 \pm 0.125$	$0.654 \pm 0.008$	$0.530 \pm 0.013$
TaF-GB	$0.717 \pm 0.011$	$0.717 \pm 0.011$	$0.147 \pm 0.006$	$0.532 \pm 0.007$	$0.484 \pm 0.001$
TaF-LGBM	$0.769 \pm 0.005$	$0.769 \pm 0.005$	$0.361 \pm 0.148$	$0.646 \pm 0.008$	$0.488 \pm 0.006$